Development of triple co-culture breast cancer spheroids for testing nanomedicines

Mariana Miranda Domingues

Mestrado Integrado em Bioengenharia

Supervisor: Doutora Flávia Castro

Co-supervisor: Professor Doutor Bruno Sarmento

September 15, 2021

© Mariana Domingues, 2021

Development of triple co-culture breast cancer spheroids for testing nanomedicines

Mariana Miranda Domingues

Mestrado Integrado em Bioengenharia

September 15, 2021

Abstract

Breast cancer is one of the most predominant cancers in the world and the most frequent in women, registering an increasing incidence rate of 0.5% every year. This, combined with the development of resistance to the currently approved therapies, raises the need to develop new therapeutic approaches to treat this disease. However, the translation of new therapies to the clinic has been hampered by the absence of cellular models that can mimic the features of *in vivo* breast tumor microenvironment. Therefore, the development of innovative 3D models able to provide consistent and predictive responses about the *in vivo* efficacy of the formulations is still an unmet preclinical need.

Taking this into consideration, the aim of this dissertation was to develop a 3D cell model based on multicellular breast tumor spheroids that combines human epithelial breast cancer cells, fibroblasts and macrophages. To characterize this triple co-culture model, the evaluation of the size and metabolic activity of the spheroids was performed overtime. Hematoxylin and eosin staining, immunohistochemistry analysis for the different cell populations and cell viability assays were also performed.

The final optimized model consisted in a spheroid seeded at an initial cell density of 5,000 cells, with the following initial ratio of MCF-7 cells to monocytes to fibroblasts – 1:2:1.

Upon successful establishment of the triple co-culture model, its validation as a platform for drug screening studies was carried out by treatment with previously optimized gefitinib (GEF)-encapsulated nanoparticles. The results showed that these nanoparticles may display, to some extent, a cytotoxic effect in the spheroids, therefore suggesting the potential therapeutic effect of the GEF-loaded nanoparticles in breast cancer treatment.

Overall, the triple co-culture spheroids developed constitute an improved model over others, as they recapitulate key features of the breast cancer microenvironment, while representing a valuable tool to more effectively predict the therapeutic effect of new treatments in breast tumor’s behavior.

Resumo

O cancro da mama é um dos tumores malignos mais predominantes a nível mundial e o mais frequente em mulheres, registando uma taxa anual de incidência crescente de 0,5%. Este aspeto, combinado com o desenvolvimento de resistência aos tratamentos atualmente aprovados para esta doença, levanta a necessidade de desenvolver novas abordagens terapêuticas para o tratamento deste cancro. Contudo, a translação de novas terapias para clínica tem sido dificultada pela falta de modelos celulares que mimetizem, de forma mais fidedigna, as características do microambiente dos tumores de mama *in vivo*. Desta forma, o desenvolvimento de um modelo 3D inovador que permita prever a eficácia *in vivo* das formulações desenvolvidas é uma necessidade clínica ainda sem resposta.

Deste modo, o objetivo desta dissertação foi o desenvolvimento de um modelo celular 3D de cancro de mama baseado em esferoides tumorais constituídos por células epiteliais de cancro de mama, fibroblastos e monócitos humanos. Para a caracterização deste modelo em tripla co-cultura, o tamanho e a atividade metabólica dos esferoides foram avaliados ao longo do tempo. Para além disso, coloração por hematoxilina e eosina, análise por imunohistoquímica das diferentes populações celulares e ensaios de viabilidade celular foram também realizados.

O modelo final otimizado consistiu em esferoides semeados a uma densidade celular inicial de 5000 células, com o seguinte rácio inicial de células – 1:2:1 (células MCF-7: monócitos:hMFs).

Após o estabelecimento bem-sucedido do modelo em co-cultura tripla, a sua validação como plataforma para o rastreio de fármacos foi realizada através do tratamento com nanopartículas encapsuladas com gefitinib. Estes resultados mostraram que as nanopartículas podem potenciar, até certo ponto, um efeito citotóxico nos esferoides, demonstrando, assim, o potencial efeito terapêutico das nanopartículas encapsuladas com gefitinib para o tratamento do cancro de mama.

No geral, os esferoides em co-cultura tripla desenvolvidos constituem uma mais-valia em relação a outros modelos, uma vez que estes mimetizam características fundamentais do microambiente tumoral do cancro de mama, constituindo também uma ferramenta valiosa para antecipar, de forma mais eficaz, o efeito terapêutico de novos tratamentos no comportamento do tumor.

Agradecimentos

Em primeiro lugar, gostaria de agradecer à minha orientadora, Doutora Flávia Castro, por toda a orientação e apoio que me deu ao longo destes meses. Também pela paciência que teve comigo e pela disponibilidade constante.

Em segundo lugar, os meus agradecimentos vão para o meu co-orientador, Professor Doutor Bruno Sarmento, por me ter aceite no seu grupo de investigação e pela sua orientação.

Também gostaria de agradecer a todas as pessoas do grupo N&TDD, do i3S, por me fazerem sentir tão acolhida e por sempre se mostrarem dispostas para me ajudar. Também à Margarida por ter sido a minha companheira de longas horas na sala de cultura.

Não podia deixar de agradecer a todas as pessoas que fizeram parte do meu percurso durante estes últimos 5 anos.

Aos amigos que conheci na faculdade, principalmente a todos os elementos do Kermit com quem passei alguns dos melhores momentos destes 5 anos. Agradecer especialmente às biotecas Luana, Nela, Chica, Miranda e Macedo que me acompanharam mais de perto nestes últimos 3 anos. Ainda temos de ir provar o tão desejado Bolo da Trofa. Um agradecimento também muito especial à Helena por todas as vezes que me acolheu em sua casa e por ser a melhor anfitriã.

Aos amigos de sempre que, mesmo estando em faculdades e cidades diferentes, continuaram a estar sempre presentes na minha vida, nomeadamente ao Fábio, à Chica, à Joana, à Rita, à Ritinha, ao Zé e ao Márcio. Um agradecimento especial ao meu feupinho preferido Gonçalo e à Sara, que me continua a acompanhar ao fim de tantos anos.

À minha família, por todo o apoio que me deram e continuam a dar. Sei que vou poder sempre contar convosco. Ao meu avô Lino e às minhas avós Céu e Paulina por serem os melhores avós que alguém poderia pedir e por se certificarem constantemente se me tenho alimentado bem. Aos meus tios Rui, Paulo, Olga, Mimi, Manuel, Nuno e Titi Diana por todos os momentos bem passados em família. Aos meus primos Alex, Maria, Lela, Simão, Mafi e Nitinha por todas as brincadeiras ao longo dos anos, pelos jantares de sushi e escape rooms. Ainda, à Titi e ao avô Zeca que vão estar sempre no meu coração e pensamento.

À minha irmã, que foi incansável comigo, principalmente nestes últimos meses em que andei mais stressada. Obrigada por tudo.

Por último, o meu maior agradecimento não poderia deixar de ser para os meus pais que estiveram sempre lá para tudo. Por me apoiaram quando estava mais em baixo, por aturarem o meu mau humor e o meu stress. Devo-vos a vocês tudo o que sou e tenho hoje. Nada do que faça ou diga será suficiente para retribuir tudo o que fazem por mim.

A todos o meu muito obrigada!

Mariana Domingues

“We are drowning in information,
while starving for wisdom.”

– Edward Osborne Wilson

Contents

Introduction 1

1.1 Context and motivation 1

1.2 Objectives and expected contributions 1

1.3 Document structure 1

Literature Review: Breast cancer 3

2.1 Overview 3

2.1.1 Anatomy of the female breast 3

2.1.2 Symptoms 4

2.1.3 Risk factors and prevention 4

2.1.4 Screening methods 5

2.2 Subtypes of breast cancer 6

2.2.1 Histological classification 6

2.2.2 Molecular classification 6

2.3 Main treatments and their limitations 8

2.3.1 Local therapy 8

2.3.2 Systemic therapy 9

2.4 The tumor microenvironment in breast cancer 11

2.4.1 Cancer-associated fibroblasts 12

2.4.2 Immune microenvironment 13

2.5 Current and emerging 3D breast cancer models 15

2.5.1 Breast cancer spheroids 15

2.5.2 Breast cancer organoids 17

2.5.3 3D bioprinting 18

2.5.4 Tumor-on-a-chip 18

Materials and Methods 19

3.1 Ethics statement 19

3.2 Human monocyte isolation 19

3.3 Cell culture 19

3.5 Multicellular tumor spheroid characterization 20

3.5.1 Size measurement ... 20
3.5.2 Metabolic activity ... 20
3.5.3 Live/dead cell assay ... 21
3.5.4 Histological analysis ... 21
3.5.5 Immunohistochemistry ... 21
3.5.6 Flow cytometry ... 22
3.6 Production of gefitinib-encapsulated PLGA nanoparticles ... 23
3.7 Characterization of the nanoparticles ... 23
3.8 Evaluation of gefitinib nanoparticles therapeutic efficacy in the established breast cancer 3D model ... 23
3.8.1 Assessment of the nanotherapeutic effect in cell viability ... 24
3.8.2 Assessment of the nanotherapeutic effect in metabolic activity ... 24
3.9 Nanotherapeutic treatment in MCF-7 2D cell culture ... 24
Results and Discussion ... 25
4.1 Development and characterization of a monoculture breast tumor spheroid model ... 25
4.2 Development and characterization of a double co-culture breast tumor spheroid model ... 27
4.3 Development and characterization of a triple co-culture breast cancer spheroid model ... 29
4.3.1 Flow cytometry characterization ... 32
4.3.2 Live/dead assay ... 33
4.3.3 Immunohistochemistry analysis ... 35
4.4 Nanoparticles production and characterization ... 36
4.5 Evaluation of gefitinib nanoparticles therapeutic efficacy in established breast cancer 3D model ... 37
Conclusion ... 45
5.1 Concluding remarks ... 45
5.2 Future perspectives ... 45
Appendix A ... 47
Appendix B ... 48
Appendix C ... 49
Appendix D ... 50
Appendix E ... 51
References ... 53

List of Figures

Figure 1 Schematic representation of the anatomy of the female breast (lateral and anterior views, from left to right). 4

Figure 2 Molecular breast cancer subtypes with the respective molecular markers and main treatments applied. 7

Figure 3 Representation of the tumor microenvironment in breast cancer, comprising different cell types, as well as several chemokines, cytokines and growth factors. 12

Figure 4 Most common scaffold-free techniques to produce multicellular tumor spheroids.... 16

Figure 5 Characterization of MCF-7 monoculture MCTS, assembled at four different initial cell densities, over seven days of culture. 26

Figure 6 Characterization of MCF-7:hMF double co-culture MCTS, assembled at the initial cell density of 5,000 cells/spheroid, over seven days of culture. 28

Figure 7 Characterization of MCF-7:monocytes:hMF triple co-culture MCTS, assembled at the initial cell density of 5,000 cells/spheroid, over seven days of culture. 31

Figure 8 MCF-7 characterization of MCF-7:monocytes:hMF triple co-culture MCTS, assembled at the initial cell density of 5,000 cells/spheroid, by flow cytometry. 32

Figure 9 Cell viability assessment of the MCTS through a live/dead assay using calcein AM and EthD-1 to stain live and dead cells, respectively. 34

Figure 10 Immunofluorescence microscopy images of mono-, double and triple culture MCTS at day 7 after cell seeding. 35

Figure 11 Evaluation of the relative metabolic activity of treated MCF-7 cells in relation to the non-treated cells (100% viability), culture in 2D, at 24 h and 48 h after treatment initiation with different therapeutic approaches. 38

Figure 12 Cell viability assessment of the 2D MCF-7 cell culture through a live/dead assay using calcein AM and EthD-1 to stain live and dead cells, respectively. 39

Figure 13 Evaluation of the relative metabolic activity of treated 3D triple culture MCTS in relation to the non-treated spheroids (100% viability) at 24 h and 48 h after treatment initiation with different therapeutic approaches. 40

Figure 14 Evaluation of the relative 3D triple culture MCTS cell activity in relation to the non-treated spheroids (100% viability) at 48 h after treatment initiation with different therapeutic approaches. 41

Figure 15 Cell viability assessment of the 3D MCTS through a live/dead assay using calcein AM and EthD-1 to stain live and dead cells, respectively. 42

Figure 16 Characterization of MCF-7:hMF double co-culture MCTS, assembled at the initial cell density of 2,500 cells/spheroid, over seven days of culture. 47

Figure 17 Detailed immunofluorescence microscopy images of mono-, double and triple culture MCTS at day 7 after cell seeding.. 48

Figure 18 Comparison study between MCF-7 monoculture MCTS seeded in different culture media at the cellular concentration of 5,000 cells/ spheroid, regarding their metabolic activity and size. 49

Figure 19 MCF-7 characterization of MCF-7:monocytes:hMF triple co-culture MCTS, assembled at the initial cell density of 5,000 cells/spheroid, by flow cytometry. 50

Figure 20 Quantitative results of the calcein AM and EthD-1 fluorescence intensities regarding different spheroid conditions measured at days 1, 4 and 7 after cell seeding. 51

List of Tables

Table 1 Information on the primary antibodies used for immunohistochemistry analysis........ 22

Table 2 Information on the secondary antibodies and DAPI solution used for immunohistochemistry analysis.. 22

Table 3 Physicochemical properties of the empty and gefitinib-loaded NPs produced. 37

Abbreviations and symbols

ACS	American Cancer Society
AI	Aromatase inhibitor
ALND	Axillary lymph node dissection
BCSC	Breast cancer stem cell
BSE	Breast self-exam
CBE	Clinical breast exam
CAF	Cancer-associated fibroblast
DC	Dendritic cell
DCIS	Ductal carcinoma *in situ*
ECM	Extracellular matrix
EGF	Epidermal growth factor
ER	Estrogen receptor
FAP-alpha	Fibroblast activation protein alpha
FDA	Food and Drug Administration
FGF	Fibroblast growth factor
FSP1	Fibroblast-specific protein 1
GEF	Gefitinib
GnRH	Gonadotropin releasing hormone
HER-2	Human epidermal growth factor receptor 2
HGF	Hepatocyte growth factor
HR	Hormone receptor
IARC	International Agency for Research on Cancer
IGF	Insulin-like growth factor
ILC	Invasive lobular carcinoma
IL-2	Interleukin-2
IL-4	Interleukin-4
IL-6	Interleukin-6
IL-10	Interleukin-10
IL-13	Interleukin-13
ISO	International Organization for Standardization
LCIS	Lobular carcinoma *in situ*
LHRH	Luteinizing releasing hormone
LPA	Lysophosphatidic acid
MCTS	Multicellular tumor spheroid
MMP	Matrix metalloproteinase
MRI	Magnetic resonance imaging
MSC	Mesenchymal stem cell
NPs	Nanoparticles
NK	Natural killer
PDGFRα/β	Growth factor receptors alpha and beta
PD-1	Programmed cell death protein 1
PDL-1	Programmed cell death ligand 1

PEG	Polyethylene glycol
PG	Prostaglandin
PGA	Polyglycolic acid
PGE2	Prostaglandin E2
PLA	Polylactic acid
PLGA	Poly (lactic co-glycolic acid)
PR	Progesterone receptor
SERM	Selective estrogen receptor modulator
SLN	Sentinel lymph node
TAM	Tumor-associated macrophage
TGF-β	Transforming growth factor β
TME	Tumor microenvironment
TNBC	Triple negative breast cancer
TNFα	Tumor necrosis factor α
TPM3	Tropomyosin 3
TxA2	Thromboxane A2
VEGF	Vascular endothelial growth factor
WHO	World Health Organization
αSMA	Alpha smooth muscle actin
°C	Degree Celsius
SD	Standard deviation
2D	Two-dimensional
3D	Three-dimensional

Chapter 1

Introduction

1.1 Context and motivation

In 2020, breast cancer was the most frequently diagnosed cancer globally and registered the fifth highest mortality rate among all cancer types [1]. Although there are approved therapies to treat this disease, the development of therapeutic resistance remains a major clinical challenge in the treatment of breast cancer patients [2]. Therefore, there is an emergent need to develop new anticancer therapeutic agents. However, in comparison to other therapeutic areas, cancer displays the lowest approval rate regarding the development of new drugs. This situation is greatly attributed to the lack of clinically relevant models that effectively reproduce the features of *in vivo* tumors and respective microenvironment [3]. Consequently, it is crucial to establish more robust models that better recapitulate breast cancer conditions, which will ultimately contribute to a higher feasibility of the results obtained on drug screening studies and favor the development of more efficient therapies to treat this disease.

1.2 Objectives and expected contributions

Taking into consideration the previous information, the main objectives of this dissertation comprehend the:

- Establishment and characterization of a 3D breast multicellular tumor spheroid (MCTS) model by combining epithelial breast cancer cells, human fibroblasts and human blood-derived macrophages;
- Validation of the developed 3D breast tumor model as a platform for drug screening through the evaluation of the therapeutic efficacy of a nano-based drug delivery system encapsulating GEF, a drug that has formerly shown promising *in vitro* results regarding breast cancer treatment [4, 5].

This work is expected to contribute to the establishment of a valuable tool to be used, in the future, for high throughput screening of different therapeutic agents that seek approval for breast cancer treatment.

1.3 Document structure

This document is divided into 5 chapters. The current chapter comprises the introduction to the work, in which a contextualization to the main problematic of the dissertation is given, as well as a clarification of the main objectives. Chapter 2 addresses the recent state of the art regarding breast cancer. Therefore, a brief explanation of the disease (including the main symptoms, risk factors, molecular subtypes and main treatments) is given, along with an overview of key cellular components, and respective roles, in the breast tumor microenvironment, followed by an elucidation of the most important 3D breast cancer models that are currently used to recapitulate this disease *in vitro*. Chapter 3 focuses on the description of the experimental methodologies performed to develop the triple co-culture breast cancer model desired, while chapter 4 is dedicated to the analysis of the results obtained regarding this model, complemented with the discussion on those same results. Finally, chapter 5 comprehends the final remarks on the dissertation, as well a brief perspective on possible future work.

Chapter 2

Literature Review: Breast cancer

2.1 Overview

Breast cancer is one of the most frequent malignant tumors worldwide, representing approximately 30% of all female cancers [6]. In fact, according to recent statistics from the International Agency for Research on Cancer (IARC), breast cancer has been overall reported as the most commonly diagnosed cancer type in 2020, accounting for an estimated number of 2.3 million new cases (11.7% of all cancer cases), thereby surpassing lung cancer. Moreover, it currently holds the fifth highest cancer mortality rate, with 685,000 deaths (6.9% of all cancer deaths) registered globally, in that same year [1, 7].

Even though the mortality rate has been declining in the past few years, mainly due to an earlier diagnosis, the incidence rate of breast cancer has been on a growing trend of 0.5% every year, according to recent statistics. This is, at least partially, attributed to an increase in body weight and a decreased fertility rate [6].

2.1.1 Anatomy of the female breast

Female breasts, located in the pectoral region, on the anterior thoracic wall, can be divided into three major structures: corpus mammae, subcutaneous tissue and the skin. The morphology of the corpus mammae can be further divided into the parenchyma (mammary gland) and the stroma [8].

The mammary glandular tissue is a specialized tissue responsible for milk production, which comprises breast lobes and lactiferous (or milk) ducts. These structures are usually where breast cancer begins its development [9, 10].

The stroma is the supporting structure of the breast that surrounds the parenchyma. It comprehends the fibrous and adipose tissues, as well as the nerves, blood vessels and lymphatics [7]. The fibrous stroma forms the suspensory ligaments of Cooper that suspend the mammary gland from the pectoral fascia, while the fatty stroma fills in the spaces between the fibrous and glandular tissues, and consequently largely dictates the size of the breasts [11].

The skin of the breast includes the areola and the nipple, as well as the general skin [8]. The nipple is a conical eminence which is connected to the several ducts. It contains smooth muscle fibers and is highly innervated with sensory nerve endings. The areola is a circular pigmented area that surrounds the nipple and is rich in sebaceous glands named tubercles of Montgomery. These glands have an important role especially during pregnancy and lactation, through the lubrification and consequent protection of both the nipple and the areola [8, 11].

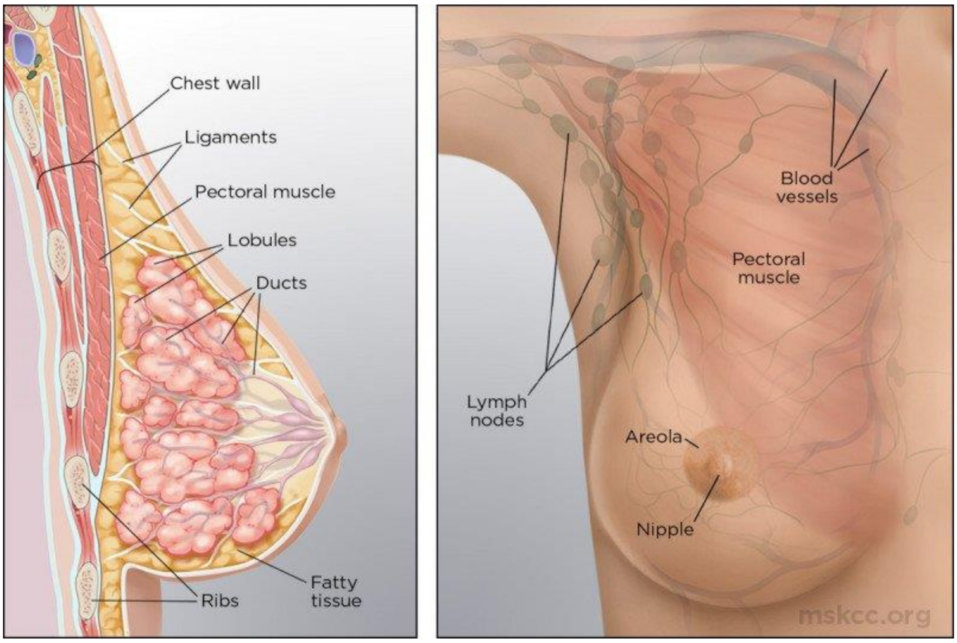

Figure 1 Schematic representation of the anatomy of the female breast (lateral and anterior views, from left to right). From [10].

2.1.2 Symptoms

Distinct people may manifest different symptoms of breast cancer, while some may not manifest any symptoms at all. Nevertheless, it is important to be aware of a number of signs that can be associated with this disease, such as [7, 12]:

- the appearance of a new lump or thickening in the breast or armpit;
- alterations of the breast concerning its size or shape;
- changes in breast skin, namely dimpling, pitting, a rash or redness of the skin, among other alterations;
- changes in the areola or in the position of the nipple;
- abnormal fluid leaking from the nipple.

2.1.3 Risk factors and prevention

Epidemiologic studies have helped establishing a variety of risks factors that are usually associated with breast cancer, which include both modifiable (such as diet, smoking habits, physical activity, etc.) and nonmodifiable factors (like gender, age, family history, among others) [13].

Out of all the aspects to take into consideration, age and gender are definitely the most crucial ones for breast cancer, as it is a disease that occurs almost exclusively in women (male breast cancer accounts for less than 1% of all breast cancers), especially after the age of 50 [14]. However, there are several other factors, including genetic or hereditary, hormonal and reproductive, as well as lifestyle factors, which can increase the possibility of developing breast cancer.

Taking in consideration the hereditary background, 20-25% of breast cancer patients have a first degree relative who has been diagnosed with this disease. Nonetheless, most genetic mutations are sporadic and only 5-10% of these cases have an autosomal dominance inheritance [13, 15]. Hereditary cancers are mainly explained by inherited mutations in the *BRCA1* and *BRCA2* genes, which play a key role in repairing double-stranded DNA breaks in the nucleus. In fact, women carrying mutations in these genes have an approximately 40-87% risk of developing breast cancer by age 70 [13].

Although genetic factors have a huge impact on a person's predisposition to this disease, breast cancer is generally a multifactorial disease, which means that non-genetic aspects have a crucial role as well [13]. For instance, it has been widely reported that an increased estrogen exposure contributes for a higher risk of developing breast cancer [16]. As such, reproductive history aspects like younger age during menarche (first menstrual cycle) and older age at menopause, are more likely to increase the risk of breast cancer. The use of contraceptive methods, as well as the use of hormone replacement therapy (HRT) after menopause constitute other hormone-related factors believed to increase this risk, according to several studies [14, 15]. Additionally, various reports have indicated that older age at first full-term pregnancy may increase the chance of breast cancer, while prolonged breastfeeding has been associated with a reduced risk of having this disease [13, 14]. Amidst the lifestyle factors, alcohol consumption, obesity, active smoking and lack of physical activity were shown to be important risk factors for the development of breast cancer [13-16].

While many of these factors correspond to aspects that one cannot control or change, it is possible to reduce the risk of breast cancer by adopting a few measures that promote a healthier lifestyle. Even with these precautions, however, the risk is only reduced by 30%, at most [7]. Therefore, it is highly recommended for women to undergo regular screening tests for early detection of breast cancer, since the 5-year relative survival rate is around 99% when breast cancer is diagnosed at an early stage, according to the American Cancer Society (ACS) [9]. In agreement with this statement, studies have shown that the breast cancer mortality rate has dropped by 41%, since 1989, mainly due to an increased implementation of screening procedures, along with improved treatment options [6].

2.1.4 Screening methods

Mammography remains the most widely used screening method in breast cancer [17]. A mammogram consists of a low-dose x-ray that produces an image of the breast tissue [9]. The ACS guidelines recommend that women with moderate risk of developing breast cancer should get a mammogram every year starting at age 45 until age 54, with the possibility of switching to a mammogram every 2 years after that age [18]. Magnetic resonance imaging (MRI) is another method that can be used to screen women for breast cancer; however, following the recommendations from the ACS, it should be used as a complementary method to screening mammography, and not as a substitute to the former.

In addition, women are encouraged to perform a breast self-exam (BSE) regularly, to check for lumps or other physical changes, as well as to become familiar with the anatomy of their own breasts [15]. Regardless, there is little evidence about its effectiveness as a screening method for breast cancer. This examination can also be performed by a healthcare professional and, in that case, it is called a clinical breast exam (CBE). In a similar way to BSE, the accuracy of this exam is questionable and its efficacy is highly dependent on the examiner's expertise [15, 19].

2.2 Subtypes of breast cancer

Breast cancer is a very heterogeneous disease that, traditionally, has been categorized based on the histological assessment of the tumor tissue [20]. However, this classification has proven to be insufficient in prognosis evaluation, as well as in predicting the response to a specific targeted therapy [20, 21]. Therefore, more recently, studies have been conducted to further analyze and characterize molecular patterns in breast cancer that can be incorporated in new classification systems for this disease [21].

2.2.1 Histological classification

Regarding the histological analysis, breast cancer can be primarily classified into *in situ* carcinoma and invasive carcinoma, which happens when tumor cells cross the basement membrane and invade the surrounding stroma [22].

Breast *in situ* carcinoma

Breast *in situ* carcinoma can be further subdivided into ductal carcinoma *in situ* (DCIS) and lobular carcinoma *in situ* (LCIS). The former is the most common type of non-invasive breast cancer and it is confined to the breast ducts, while the latter is limited to the breast lobes [23]. DCIS may additionally be categorized into one of five subtypes, according to the architectural features of the tumor: papillary, micropapillary, comedo, cribriform and solid [21, 22].

Breast invasive carcinoma

Invasive tumors are also a very heterogeneous group, with over 20 subtypes defined by the World Health Organization (WHO) [20, 22, 24]. The most frequent of them is invasive ductal carcinoma of no special type (IDC-NST), which accounts for approximately 40-75% of the cases [22]. IDC refers to a cancer that has its origin in the milk ducts but has spread into the surrounding breast tissue. The classification of “no special type” relates to the fact that these tumors have very distinctive morphological characteristics, and thereby do not gather enough common features to be categorized into a histological “special type” [25]. The diagnosis of this type of cancer is assessed through an exclusion method, when the histological characteristics of the tissue do not fulfill the criteria for any histological special subtype [20].

Amidst the special types, the more commons include invasive lobular carcinoma (ILC), which is the second most prevalent type of invasive breast carcinoma, as well as ductal/lobular, medullary, tubular, mucinous and papillary carcinomas [22]. Other rarer breast carcinomas comprise inflammatory breast cancer, Paget’s disease of the breast and phyllodes tumor [23].

2.2.2 Molecular classification

Another classification system for the assessment of breast cancer subtypes is based on the molecular patterns of the tumor tissue, which provide a better prognostic value than the classic histological division. In particular, breast cancers can be divided according to the presence or absence of three molecular receptors: estrogen receptor (ER), progesterone receptor (PR) and human epidermal growth factor receptor 2 (HER2) (Figure 2) ([22].

ER and PR are hormone receptors that are expressed in several breast cancers. These receptors have an important role in tumorigenesis through the binding to the respective hormones (estrogen and progesterone), which activates mechanisms that lead to uncontrolled cell division and ultimately result in cancer growth [26]. HER2 is a membrane tyrosine kinase that is involved in signaling pathways that also promote cell proliferation and survival. It is overexpressed in about 20% of breast cancers [27]. Furthermore, Ki67 is a cell proliferation marker that can additionally be used to help distinguishing between the different molecular subtypes, especially luminal A and luminal B carcinomas [28].

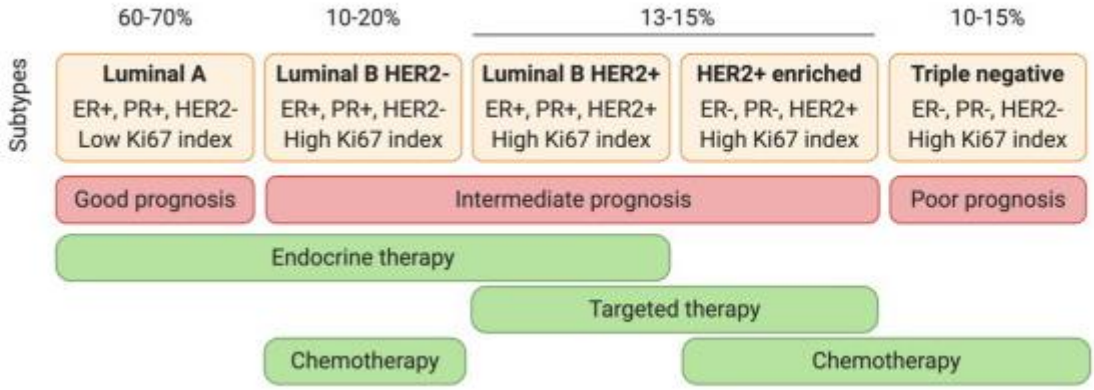
60-70%
10-20%
13-15%
10-15%
Subtypes
Luminal A
ER+, PR+, HER2-
Low Ki67 index
Luminal B HER2-
ER+, PR+, HER2-
High Ki67 index
Luminal B HER2+
ER+, PR+, HER2+
High Ki67 index
HER2+ enriched
ER-, PR-, HER2+
High Ki67 index
Triple negative
ER-, PR-, HER2-
High Ki67 index
Good prognosis
Intermediate prognosis
Poor prognosis
Endocrine therapy
Targeted therapy
Chemotherapy
Chemotherapy

Figure 2 Molecular breast cancer subtypes with the respective molecular markers and main treatments applied. Adapted from [29].

Taking this into consideration, breast cancers can be alternatively divided into [25, 30]:

Luminal A – ER-positive, high levels of PR, HER2-negative and low expression of Ki67. This is the most frequent subtype, accounting for nearly half of the diagnosed cases. Moreover, it tends to grow slowly and it is generally associated with the most favorable prognosis.

Luminal B – this subtype can be subcategorized into luminal B, HER2-negative and luminal B, HER-2 positive. Besides the levels of HER2, there are other molecular differences regarding these subcategories. The former is ER-positive and presents low levels of PR but high levels of Ki67. The latter is also ER-positive but may present high or low levels of Ki67 and PR. Luminal B cancers represent 20-30% of newly diagnosed breast cancer cases and, in comparison to luminal A tumors, have a poorer prognosis and a faster-growing tendency.

HER2-enriched – opposite to luminal A and luminal B, which are both hormone receptor-positive carcinomas, HER2-enriched is classified as a hormone receptor-negative subtype (that is, ER and PR-negative). It is characterized by high expression levels of HER2 and comprises 15-20% of breast cancer cases. Studies have shown that HER2 overexpression correlates to a higher proliferative capacity of the tumors and propensity to metastasis, therefore being associated with a worse prognosis than the subtypes mentioned above.

Triple negative – triple negative breast cancer (TNBC) is considered the most aggressive subtype of breast cancer, accounting for 10-20% of all cases. It is defined by the lack of expression of all three molecular receptors – ER, PR and HER2. Importantly, a correlation between this subtype of cancer and mutations in the *BRCA1* gene has been well-described, with

70% of breast cancers that harbor a mutation in this gene presenting a triple-negative phenotype [30, 31].

Some literature additionally reports the existence of a fifth subtype referred to as “normal-like”. Though very similar to the luminal A subtype in terms of expression patterns, it is characterized by a comparably worse prognosis [30, 32].

2.3 Main treatments and their limitations

Because of breast cancer’s heterogeneity, the therapeutic options to be applied in each situation may vary and are highly dependent on the stage of the disease and the molecular breast cancer subtype [7].

In case of nonmetastatic breast cancer, treatment should be aimed at locally eliminating the tumor (usually through surgery and radiation therapy) and preventing the risk of metastatic spread using systemic therapy, such as hormonal therapy, chemotherapy and targeted therapy [7, 33]. In regards to metastatic breast cancer, therapeutic approaches focus on prolonging life and providing palliative care [33].

2.3.1 Local therapy

Surgery

In the past, mastectomy, which consists in the complete removal of the breast, was considered the standard surgical treatment for breast cancer [34]. Today, however, most of the breast surgeries carried out result from a smaller procedure, called lumpectomy or breast-conserving surgery, in which only the tumor and a small margin of healthy tissue are resected from the breast [7, 35]. Following this surgical intervention, radiation therapy is usually recommended, in order to prevent the chance of relapse [7].

Another surgical treatment that is often performed along with mastectomy or lumpectomy in invasive carcinomas is axillary lymph node dissection (ALND), which is the removal of lymph nodes, from under the arm, that drain the breast tissue [35]. This procedure is used not only as a therapeutic tool (to remove cancer cells and, consequently, prevent the spread of the tumor), but also in diagnosis (to determine the invasiveness level of the cancer) [33]. Yet, it can cause pain, swelling, numbness and lack of mobility in the operated arm. Due to this, in case of no clear evidence of cancer in the lymph nodes, ALND has often been replaced with a smaller intervention – called sentinel lymph node (SLN) biopsy – that only removes a few lymph nodes, thus reducing the side effects associated with the former procedure.

Even though surgery is usually the first line of treatment against breast cancer, not all tumors can be removed with surgery. Furthermore, a surgical procedure is not generally performed alone, but rather is combined with other approaches that are applied before or after surgery, as neoadjuvant or adjuvant therapies, respectively [7].

Radiation therapy

Radiation therapy, or radiotherapy, is characterized by the use of high energy x-rays to destroy cancer cells. It is usually delivered as external beam radiation, but it can also be given as brachytherapy (or internal radiation), in which the source of radiation is placed inside the body, within the tumor or close to it [36].

Radiotherapy is usually given after mastectomy or lumpectomy, as an adjuvant therapy to prevent relapse, with reported data showing a decrease by nearly half in breast cancer recurrence at 10 years [36, 37]. It may be applied to the entire breast or only to a portion (after lumpectomy), to the chest wall (in the case of mastectomy) and to the regional lymph nodes [33]. Though more uncommon, radiotherapy can also be delivered as a neoadjuvant therapy to shrink a tumor that is very large to be removed by surgery. In addition, it can be applied in metastatic breast cancer (bone, liver, lung, brain metastasis, for instance) [38]. However, this therapy is associated with side effects, such as swelling in the breast, fatigue and skin changes in the area exposed to the radiation (redness of the skin, discoloration, pain, burning or peeling) [38].

2.3.2 Systemic therapy

Hormonal therapy

Hormonal (or endocrine) therapy is the standard systemic treatment for hormone receptor-positive tumors, such as luminal A and luminal B subtypes [33]. This therapeutic approach acts by blocking estrogen's action on breast cancer cells (antiestrogen), or by lowering its levels in the body [34]. The most common medicines used for these purposes are tamoxifen and aromatase inhibitors (AIs) (such as anastrozole, letrozole and exemestane), respectively. They are usually administered orally for 5 to 10 years and should be considered according to menopausal status [7, 33].

Tamoxifen is a selective estrogen receptor modulator (SERM) that, in breast cells, acts as an estrogen antagonist (antiestrogen) by competing with this hormone for ER binding [33]. This prevents estrogen from interacting with breast cancer cells, which, in turn (considering estrogen's proliferative properties), inhibits uncontrolled cell division and cancer growth. This drug works effectively both in pre- and postmenopausal women [33, 39]. Side effects of tamoxifen include hot flashes, as well as vaginal discharge, dryness or bleeding [38]. AIs, on the other hand, promote the reduction in circulating estrogen levels by inhibiting aromatase's activity, which is an enzyme responsible for converting androgens into estrogens. Opposite to tamoxifen, AIs are only effective in postmenopausal women. [33, 38]. Muscle and joint pain/stiffness, hot flashes and higher risk of osteoporosis are some adverse effects associated with this therapy [38].

Furthermore, ovarian ablation or suppression are other hormonal therapeutic options that can be applied to pre-menopausal women. The former consists in surgically removing the ovaries, which are the main producing sources of estrogen. However, it is an irreversible approach that can lead to serious side effects, so it is not very commonly used. The latter comprehends the use of drugs, like luteinizing or gonadotropin releasing hormone (LHRH or GnRH) agonists, to inhibit estrogen production by the ovaries [40]. Since neither of these approaches can treat breast cancer on their own, they are usually combined with tamoxifen or an aromatase inhibitor [38].

Endocrine therapy is usually given as an adjuvant therapy, but it can also be used as a neoadjuvant treatment. One of the major clinical challenges regarding this therapy is the development of *de novo* and acquired resistance to treatment by the patients. In order to try to overcome this issue, endocrine therapy is sometimes combined with chemotherapy, though with arguable benefits [41]. Moreover, it is only effective in hormone receptor-positive breast cancers, so it is not helpful in the treatment of HER2-enriched and triple negative breast cancer subtypes [34].

HER2-targeted therapy

For the treatment of HER2-enriched breast cancers, one of the major advances was the development of targeted biological agents, such as monoclonal antibodies that specifically target the HER2 protein. Another therapeutic approach that can be applied to this subtype is the administration of protein tyrosine kinases inhibitors [33].

The most common monoclonal antibody used in HER2-enriched cancer is trastuzumab, which targets the extracellular domain of HER2 [33]. Though it can be administered alone, trastuzumab is usually combined with anthracyclines and paclitaxel chemotherapy. In fact, due to overall great outcomes and reduced toxicity, paclitaxel/trastuzumab is currently considered the standard treatment for patients with small/node-negative HER2-positive tumors. However, it is important to acknowledge that the administration of trastuzumab and anthracyclines combined may lead to heart damage in 2-3% of the patients [33, 34]. Pertuzumab is another monoclonal antibody that was approved, in combination with trastuzumab and chemotherapy, for the treatment of stage II and III breast cancer patients [38]. This antibody targets the HER2 dimerization domain and, when added to the treatment, it was shown to further reduce the risk of cancer recurrence in comparison to the standard trastuzumab-containing regimens [33]. A major drawback of therapies that use monoclonal antibodies is the cost, since these biological agents are very expensive [7].

Neratinib is a protein tyrosine kinase inhibitor of several receptors of the HER family, including HER2 [28]. It has been approved by the Food and Drug Administration (FDA) for the treatment of advanced or metastatic HER2-positive breast cancer patients who have priorly undergone at least two anti-HER2 based regimens [42]. Another kinase inhibitor which is used for metastatic HER2-positive breast cancer is lapatinib. This agent, which is a reversible blocker of HER2 protein, is used together with letrozole when patients develop resistance to trastuzumab [22].

Chemotherapy

Chemotherapy is a treatment based on administrating drugs to patients so as to weaken cancer cells and ultimately destroy them. It can be given either as a neoadjuvant therapy, to shrink the tumor, or as an adjuvant therapy, to reduce the risk of recurrence. Furthermore, it can be used in the treatment of both early-stage and advanced-stage breast cancers [38, 43].

Despite the underlying risks and limited efficacy associated with this approach, chemotherapy is considered the standard systemic therapeutic option for triple negative breast cancer treatment (though patients frequently relapse) [33, 44]. Moreover, it is rather often combined with hormonal and HER2-targeted therapies for treating hormone receptor-positive and HER2-enriched breast cancer subtypes, respectively, especially in later stages of the disease [33].

Some of the most common chemotherapeutic drugs comprise anthracyclines (like doxorubicin and epirubicin), taxanes (paclitaxel and docetaxel, for instance), platinum agents (such as cisplatin or carboplatin), 5-fluorouracil (5-FU), among others. These drugs can be administered alone, but are frequently combined together in the same treatment. Adverse effects of chemotherapy commonly consist of hair loss, weight changes, nausea, diarrhea, etc. [38, 45].

Considering this, nanomedicine is an emerging form of therapy that focuses on alternative drug delivery and improvement of the treatment efficacy while reducing detrimental side effects to normal tissues [46, 47]. Indeed, the use of drug-encapsulated nanosystems comprises several advantages over the free administration of the drug, since nanostructured delivery carriers enhance solubility and allow for a more controlled release of the drug, while also conferring protection to degradation. Consequently, the drug’s half-life and bioavailability increase and, therefore, a lower dose is required to achieve the desired therapeutic effect, which leads to less toxicity and reduced side effects [48, 49].

Although chemotherapy allows the disruption of regulatory pathways that enhance tumor growth and survival, its action is often limited by the development of mechanisms of drug resistance by cancer cells. Therefore, new therapeutical approaches combining chemotherapy and immunotherapy (commonly known as chemoimmunotherapy) have been developed as a way to overcome this issue.

Immunotherapy

Immunotherapy is a type of targeted biologic therapy that stimulates the patient’s own immune system to recognize and fight infections and other diseases, like cancer [50]. Examples of immunotherapy in breast cancer include monoclonal antibodies, such as immune checkpoint inhibitors. These drugs are capable of blocking immune checkpoint molecules, which modulate the amplitude and duration of immune responses and maintain self-tolerance, thus preventing exacerbated immune reactions and autoimmunity [51, 52].

Approved immune checkpoint inhibitors to treat breast cancer include pembrolizumab (Keytruda) and atezolizumab (Tecentriq). The former acts as an inhibitor of programmed cell death-1 (PD-1), a protein that can be found on the surface of activated T cells [50, 51]. The interaction between PD-1 and one of its ligands, PD-L1, leads to the suppression of T cell activity, which results in the downregulation of immune response mechanisms. As such, the blockage of this receptor contributes to the enhancement of the immune response against breast cancer cells. The latter is a PD-L1 inhibitor whose function is to block PD-L1, a protein that is expressed on a variety of tumor cells (including TNBC), as part of a mechanism to escape anti-tumor immunity [50, 53]. Both Keytruda and Tecentriq are approved in combination with chemotherapeutic agents to treat unresectable triple-negative, PD-L1 positive breast cancer. Possible side effects of this therapy comprise cough, nausea, fatigue, diarrhea, etc., though it can more rarely lead to autoimmune reactions [50, 54].

2.4 The tumor microenvironment in breast cancer

Over the years, the tumor microenvironment (TME) has gained significant importance as a critical player in breast cancer progression and as a therapeutic target for this disease, since stromal cells are genomically more stable than cancer cells [55]. It comprises several cell types, including fibroblasts, adipocytes, leukocytes, endothelial and myoepithelial cells, as well as components of the extracellular matrix (ECM) and soluble factors, such as growth factors, hormones and cytokines [56] (Figure 3). Here, two of the most important TME constituents will be highlighted: cancer-associated fibroblasts (CAFs) and tumor-associated macrophages (TAMs).

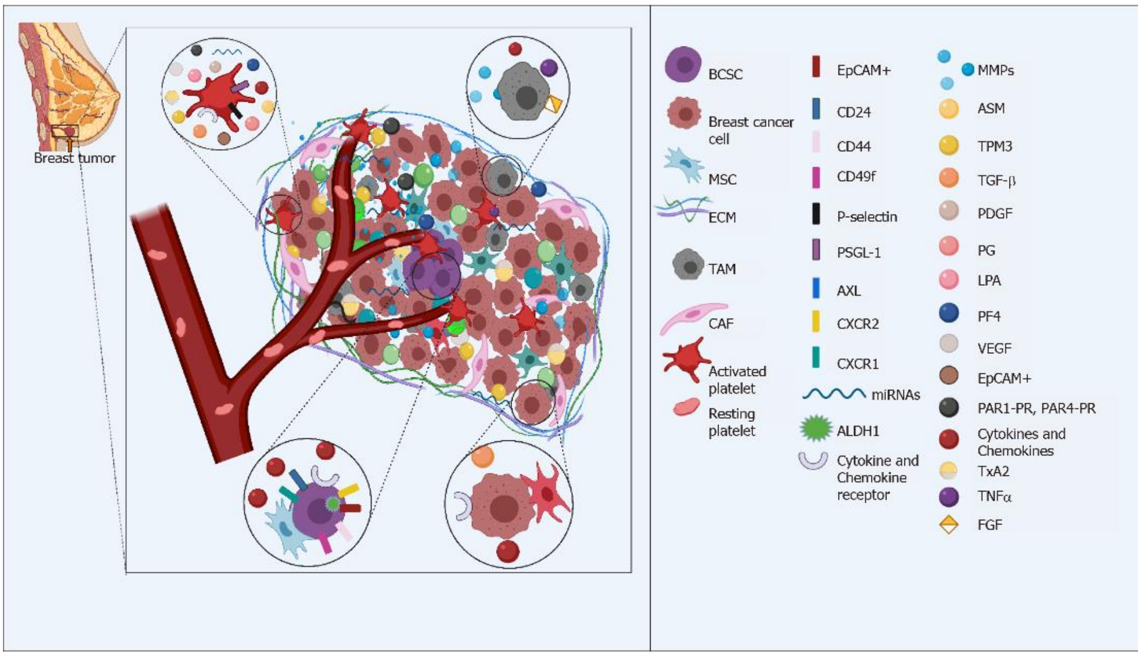

Figure 3 Representation of the tumor microenvironment in breast cancer, comprising different cell types, as well as several chemokines, cytokines and growth factors. BCSC: Breast cancer stem cells; MSC: Mesenchymal stem cell; ECM: Extracellular matrix; TAM: Tumor-associated macrophage; CAF: Cancer-associated fibroblast; EpCAM: Epithelial cell adhesion molecule; PSGL-1: P-selectin glycoprotein ligand 1; ALDH1: Aldehyde dehydrogenase 1; MMPs: Matrix Metalloproteinases; TPM3: Tropomyosin 3; TGF-β: Tumor growth factor 3; PDGF: Platelet-derived growth factor; PG: Prostaglandin; LPA: Lysophosphatidic acid; PF4: Platelet factor 4; VEGF: Vascular endothelial growth factor; PAR1-PR: Protease-activated receptor-1-PR; TxA2: Thromboxane A2; TNFα: Tumor necrosis factor α; FGF: Fibroblast growth factor. From [57].

2.4.1 Cancer-associated fibroblasts

CAFs constitute the majority of stromal cells within breast tumors [58]. Even though the origin of these cells – and whether it differs according to the breast cancer subtype – is still not fully elucidated, distinct cell types have been reported as likely precursors of CAFs, including normal tissue-resident fibroblasts and mesenchymal stem cells (MSCs). Accordingly, studies in breast cancer have shown that these cells differentiate into CAFs or CAF-like cells upon the secretion, by tumor cells, of certain soluble factors, and other components, including transforming growth factor beta 1 (TGF-β1), Wnt7a, osteopontin, miR-105 and prostaglandin E2 (PGE2), among others. Another possible source of CAFs is believed to arise from the trans-differentiation of adipocytes, pericytes, epithelial and endothelial cells present in the breast [58, 59].

Some of the markers that are usually associated with the CAF phenotype include fibroblast activation protein alpha (FAP-alpha), fibroblast-specific protein 1 (FSP1), platelet-derived growth factor receptors alpha and beta (PDGFRα/β) and alpha smooth muscle actin (αSMA). However, none of these markers are specific to this type of cells, but can also be found in normal fibroblasts, or even in immune and endothelial cells, pericytes or MSCs. Moreover, it is believed that different CAF subtypes may coexist in the same tumor and that each subpopulation can affect cancer progression in distinct ways [58].

As previously mentioned, tumor cells stimulate stromal cell transformation into CAFs. However, considerable evidence suggests that CAFs also play a fundamental role in tumor growth, invasion and metastasis [60]. For instance, it has been reported that fibroblasts found in the breast TME contribute to cancer progression by secreting high levels of stromal cell derived factor 1 (SDF-1, CXCL12). This chemokine binds to the CXCR-4 receptor present in cancer cells, which consequently activates mechanisms associated with tumor growth. Furthermore, SDF-1 is believed to recruit endothelial progenitor cells into the tumor, thereby promoting angiogenesis [61]. According to several studies, CAFs are also responsible to produce various growth factors that take part in signaling pathways that promote cancer cell survival and proliferation. Those factors include basic fibroblast growth factor (bFGF), hepatocyte growth factor (HGF), insulin-like growth factor (IGF) and epidermal growth factor (EGF) [60]. Additionally, it is important to highlight the role of TGF-β signaling as a crucial player in tumor-stroma crosstalk: while TGF-β1 is primarily secreted by tumor cells – leading to the activation of CAF-precursors –, activated CAFs, later on, also initiate TGF-β1 production, therefore ensuring continuous autocrine mechanisms of CAF activation and immune response suppression [58, 62].

Moreover, a wide variety of studies suggest that CAFs contribute to therapeutic resistance against the majority of therapies used in breast cancer treatment, including chemotherapy and endocrine therapy. Particularly, soluble factors secreted by CAFs, such as interleukin 6 (IL-6), as well as matrix metalloproteinases (MMPs) and fibronectin, were correlated to decreased sensitivity to tamoxifen in breast cancer cells [63-65]. Another very important aspect to take into consideration is that CAFs are able to modulate the TME in order to create immunosuppressive conditions that contribute to cancer progression. Importantly, CAFs synthesize cytokines and other inflammatory mediators (such as CCL12, IL-6, IL-8, CXCL1, CSF-1, TGF-β1, among others) that are involved in recruiting monocytes and driving their differentiation into immunosuppressive M2-like macrophages, promoting T-regulatory cell (Treg) differentiation and contributing to T helper 1 (Th1) cell shift into Th2 phenotype [66-70]. CCL12, for instance, is a well-known chemokine secreted by CAFs that attracts monocytes, thus allowing their infiltration into the primary tumor and metastatic sites [58]. Consequently, this crosstalk between fibroblasts present in the TME and immune cells may represent an important tool to further understand this disease and ultimately develop new therapeutic approaches to treat breast cancer.

2.4.2 Immune microenvironment

The immune microenvironment has also been increasingly recognized for its importance in overall cancer development. Indeed, the different immune cell populations that surround the tumor play a critical but distinctive role in its initiation and progression. While populations like Th1 cells, natural killer (NK) and cytotoxic T cells have been associated with a more favorable prognosis, due to their anti-tumor properties; Treg cells, M2-like macrophages and Th2 cells enable the establishment of immunosuppressive conditions within the tumor, correlating with poor clinical outcomes.

In the past, breast cancer was generally not considered a highly immunogenic type of cancer. However, in recent years, it has become clear that the level of immune infiltration – and consequently the tumor's susceptibility to immunotherapy – differs according to the BC subtype: in general, hormone receptor-positive (HR+) carcinomas are classified as immunologically "cold tumors", while HER2-enriched and TNBC are characterized by higher immune cell infiltration [71, 72]. Nevertheless, studies have reported that a subset of luminal breast cancers possess a significant percentage of infiltrating immune cells within their microenvironment [71]. Hence, the presence and relative proportion of the different immune cell populations is highly variable, which is consistent with the underlying heterogeneity of this disease. For instance, NK cells and neutrophils are commonly found in large proportions within ER-positive breast carcinomas, whereas CD4$^+$ Th cells and CD8$^+$ cytotoxic T cells are usually present in much lower concentrations. On the other hand, ER-negative breast tumors are mainly infiltrated by Treg cells, activated mast cells and M2-like TAMs, though they also incorporate dendritic cells (DCs), B lymphocytes and T cells in smaller percentages. HER2-positive cancers, in turn, are often characterized by the presence of Treg cells, neutrophils, mast cells and DCs [73]. Of note, higher immune infiltration has been particularly correlated to a better response to chemotherapy, and to overall greater clinical outcomes, especially in HER2-enriched and TNBC subtypes [74, 75].

Tumor-associated macrophages

Although their abundance varies depending on the cancer type, TAMs can be found in the majority of the tumors. Particularly, TAMs constitute a major cell population in the breast cancer microenvironment, occasionally comprising up to 50% of the tumor cell mass [53,54]. TAMs originate either from circulating monocytes that are attracted into the tumor by growth factors and chemokines (such as CCL2 and CCL5) secreted by neoplastic and stromal cells, or from tissue-resident macrophages [56, 76]. Upon stimulation with monocyte colony stimulating factor (M-CSF), recruited monocytes first evolve into non-polarized (M0) macrophages. Afterwards, these cells differentiate into one of the two main polarized phenotypes – M1-like or M2-like macrophages –, depending on the signals released from the microenvironment [76, 77].

Classically activated M1-like macrophages correspond to the predominant phenotype found in immunological responses [56]. They are stimulated by Th1 cytokines, such as tumor necrosis factor (TNF) and interferon-γ (IFN-γ), and show important anti-tumor features through the secretion of pro-inflammatory cytokines, like TNF and IL-2, as well as reactive nitrogen and oxygen intermediates [77]. On the contrary, alternatively activated M2 macrophages are associated with Th2 cell cytokines, including IL-4, IL-10 and IL-13, and display tumor-promoting properties by inhibiting phagocytosis, stimulating angiogenesis (through the secretion of vascular endothelial growth factor, VEGF) and by suppressing CD8+ T cell activity [77, 78]. The later occurs because M2 macrophages: (i) produce chemokines (namely CCL22), recruiting Treg cells which dampen effector T cell responses; and (ii) overexpress of cyclogenase-2 (COX-2), which subsequently leads to an increased expression of IL-10, an anti-inflammatory cytokine that suppresses the activation of cytotoxic T cells and IFN-γ production [56, 77]. In addition, the M2 phenotype is believed to be implicated in tissue remodeling through the release of proteolytic enzymes that degrade the ECM. As such, these cells have been often linked to the formation of metastasis, enabling tumor cell invasion to the surrounding tissue and blood vessels [56].

Importantly, M2-like macrophages correspond to the dominant TAM phenotype in breast cancer [77, 79]. As a consequence, several studies have hypothesized that a higher level of TAM infiltration correlates with a poorer prognosis in this type of cancer, which explains the increasing interest in using these cells as a therapeutic target for the treatment of this disease [56]. Most of the TAM-targeting therapies currently being explored revolve around preventing macrophage recruitment and survival; however, promising new approaches may focus on inducing a shift from the tumor-promoting M2 phenotype into the M1 tumor-suppressing profile [78].

Considering the preponderant role that the TME holds in cancer progression, it seems relevant to try to mimic, as much as possible, these interactions in the models that are currently used for the study of breast cancer. Therefore, more complex models that include different cell types found in the TME are currently drawing increasing attention.

2.5 Current and emerging 3D breast cancer models

Despite the significant advances that have been made in the understanding of breast cancer biology, there are still several aspects regarding this disease that require further investigation, which will allow the development of new treatments, and ultimately improve the survival rate of the patients. In this regard, breast cancer models act as an important tool to better recapitulate the complexity of the tumor – thus enabling more accurate studies on the mechanisms that lead to this disease –, while also contributing as valuable platforms to test new therapeutic approaches.

Currently, cancer holds the lowest approval rate of new drugs in comparison to other therapeutic groups. Accordingly, only a small percentage (less than 10%) of the newly developed oncology drug candidates that go into phase I clinical trials end up being approved by the FDA. One of the major reasons that justifies this situation is the lack of clinically relevant models that more accurately mimic tumor conditions, which consequently hampers the translation of the research done in the laboratory into the clinic. As the process of drug development is very expensive and time-consuming, there is an urgent need for the refinement of pre-clinical models that could then be used as reliable platforms for drug screening [3, 80].

For many years, conventional bidimensional (2D) cell culture systems have been the most widely used *in vitro* cancer models to study tumorigenesis and new therapeutic agents. In breast cancer, this tendency has also been verified, with the majority of the initial studies primarily involving simple methodologies, such as single tumor cell line monolayers or trans-well systems [81]. Though 2D models comprise a few advantages, such as simplicity, reduced cost, easy handling and wide availability, they lack other important characteristics. For instance, these models fail to recapitulate inter- and intra-tumor heterogeneity, and are particularly more susceptible to pharmacological action, thus limiting their ability to precisely predict the tumor's response to therapy [81, 82]. On the other hand, animal models, though extremely important as the final step before entering phase I clinical trials, are expensive to maintain and require a significant amount of time to develop. Moreover, their genomic and immune profiles are distinct to those of humans and there are several ethical issues concerning their use [3, 81].

Consequently, 3D models have gained increased recognition as they better recapitulate several hallmarks of solid tumors when compared to 2D culture systems (such as cell-cell and cell-ECM interactions, as well as hypoxic conditions that result from the heterogeneity in nutrients and O_2 perfusion), while also enabling a reduction in the use of animal models, which, in turn, should only be used to validate reliable *in vitro* data. The latter can contribute to an overall reduction in the costs and length of the drug discovery process [3, 82]. Therefore, 3D culture systems models have emerged to fill the gap between 2D monolayer cell cultures and *in vivo* tumor models.

The most well described 3D breast cancer models include organoids and spheroids, as well as 3D bioprinting approaches and organ-on-a-chip microfluidic devices.

2.5.1 Breast cancer spheroids

MCTS are 3D cell clusters formed through self-assembly or forced growth of single cell suspensions [83]. In the past, the majority of these structures comprised a single cell type (monotypic spheroids); however, more complex MCTS constituted by more than one cell type (heterotypic spheroids) have been developed since then [84].There are different techniques that enable the generation of these structures, including scaffold-based and scaffold-free approaches [29].

The former comprises the seeding of cell suspensions onto synthetic or natural matrices that mimic ECM. The most commonly used natural scaffolds include polymeric matrices based on elastin, gelatin, collagen, hyaluronic acid or Matrigel. Synthetic matrices, which allow a better control of the scaffold's properties, comprise polyglycolic acid (PGA), polylactic acid (PLA) and polyethylene glycol (PEG), among others [29, 85]. While the incorporation of scaffolds into the 3D models intends to recapitulate the ECM characteristics and mimic cell-matrix interactions, they may negatively influence cell-cell interactions and hinder cell growth. Furthermore, the fact that scaffold concentrations are constant, instead of concomitantly increasing with the growth of the structures, can compromise the growth kinetics of the spheroids [86]. In terms of validation of the model for drug screening applications, the rigidity of the ECM component may additionally hamper the drug's penetration into the structure [87].

Scaffold-free techniques – namely the hanging-drop method, the liquid overlay (LOT) technique, the agitation-based technique using spinner flasks and the magnetic culture levitation – constitute the most frequently implemented methods for spheroid formation (Figure 4) [29, 83]. The hanging-drop method consists in suspending a cell liquid drop on a coverslip, leading to spheroid aggregation caused by surface tension forces. The LOT technique relies on seeding cells on non-adhesive surfaces, such as agar or agarose, to prevent cell attachment. The generation of spheroids using spinner flasks occurs by continuously stirring cells suspensions, thus avoiding their adherence to the surfaces and, consequently, promoting their aggregation [82, 83]. Finally, the magnetic levitation technique contributes to spheroid formation through the incorporation of magnetic nanoparticles by the cells, after which external magnetic forces are applied to overcome the gravitational force, thereby concentrating the cells and inducing their aggregation into 3D spheroids [82, 85]. Even though scaffold-free strategies do not promptly recapitulate cell-matrix communication, this issue can be overcome by adding cells to the MCTS that produce elements of the ECM, namely fibroblasts. This strategy can be beneficial over the use of scaffolds since ECM concentration would not be static, but would rather increase overtime, along with the growth of the spheroids [86].

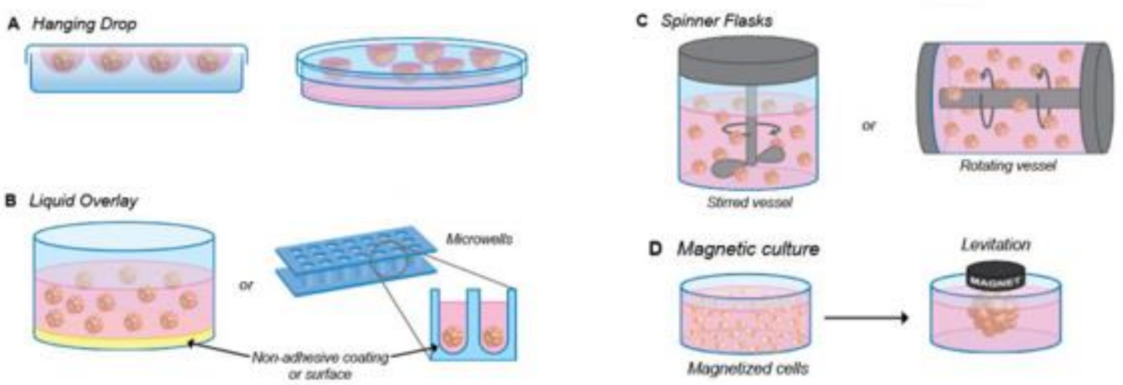

Figure 4 Most common scaffold-free techniques to produce multicellular tumor spheroids. Adapted from [85].

Spheroids closely reproduce several features of *in vivo* solid tumors, including the spatial organization, as well as the O_2 and nutrient gradients generated by impaired diffusion of these molecules along the structures, which leads to hypoxia and necrosis. Moreover, an increase in the acid lactic fermentation caused by these conditions promotes the acidification of the inner areas of the MCTS, which translates into a decrease in the pH to values around 6.2-6.9, similarly to what is observed in *in vivo* solid tumors [82, 85].

Taking this into consideration, MCTS are physiologically relevant models to characterize avascular solid tumors beyond a critical size value of about 400-500 µm, as they exhibit three heterogeneous layers of cells: an external proliferating cell layer, an intermediate zone constituted by cells in a quiescent state and an inner necrotic core [82, 85]. MCTS have also been reported to share similarities with solid tumors in terms of growth kinetics, chemoresistance and metabolic rates [82]. Furthermore, the addition of different cell types that are present in TME, such as fibroblasts and macrophages, contributes to the establishment of a more robust model to study this disease [3]. Besides the advantages mentioned above, spheroids are easier to manipulate and are associated with lower costs than organoids, making them more suitable for high throughput drug screening studies [3].

Nonetheless, while MCTS constitute an advantage over more simplistic 2D models, they also comprise a few drawbacks. Particularly, spheroids are often cell-line derived structures, thus suffering from clonal selection. This contributes to a less accurate representation of intra- and inter-tumor heterogeneity. However, this issue can be surpassed through the use of tumor-specific cells derived from primary tissue, similarly to what happens in organoids [29].

2.5.2 Breast cancer organoids

Organoids have originally been defined as self-organized 3D multicellular structures that mimic various functional and structural aspects of their corresponding *in vivo* organ [88, 89]. These structures can arise from embryonic or induced pluripotent stem cells, as well as from tissue-resident adult stem cells present in several organs [88].

Organoid structures have been established for a variety of healthy tissues, as well as patient-derived tumors, including breast cancer [3, 90]. This technique comprises several positive aspects, such as the fact that it can recapitulate the heterogeneity and spatial architecture of the original tumor. Moreover, organoids are not affected by strong selection, unlike cell lines, and they can derive from tumors at different stages, thus enabling a wider representation of the disease. Importantly, organoids can be propagated *in vitro* and cryopreserved, enabling the generation of a biobank that comprises organoids from a significant number of patients [3, 29].

Although a very powerful tool for preclinical studies, organoids are also associated with some drawbacks. For instance, one of the most common methods to generate organoids relies on submerging the cells in a dome of Matrigel, a solubilized basement membrane originated from mouse sarcoma [91]. Aside from the underlying ethical issues, the use of this substance has been controversial due to the presence of xenogeneic contaminants and because its components are variable and undefined, leading to batch-to-batch variation and subsequent lack of reproducibility of the results. Consequently, synthetic alternatives to this material have been studied [92]. Moreover, the use of a scaffold may negatively influence cell-cell interactions and hinder cell growth, as previously discussed. Also, in comparison to other models, such as spheroids, they constitute more expensive and time-consuming models to develop [3].

The two previously described models can be further improved by using other techniques that lead to the formation of more complex 3D structures that better recapitulate breast tumor conditions. As such, recent studies have increasingly focused on combining organoids and spheroids with promising methods, such as 3D bioprinting and microfluidics.

2.5.3 3D bioprinting

3D bioprinting is a promising technique that has been increasingly applied to this field. Its process consists in the layer-by-layer deposition of materials, called bioinks, to form computer-controlled 3D structures [81]. Bioinks are composed of biomaterials that can simultaneously be printed and promote cell growth and survival [84]. These materials are deposited on a matrix, which is either discarded after formation of the 3D structure, or preserved into the model, thus corresponding to a scaffold-free or to a scaffold-based approach, respectively [29].

Several recent studies have applied this technique to form 3D breast models, for example through the creation of human mammary organoids inside 3D collagen matrices or the fabrication of gelatin arrays to seed and produce MCF-7 tumors spheroids [81].

One of the major advantages of this method over others is related to its underlying ability to precisely control the location and organization of the cells that are part of the model, as well as the stiffness and biochemical composition of the structure [29, 81]. 3D printing can also be used in studies regarding breast cancer metastasis in other tissues, such as bone. Moreover, it enables the fabrication of models that mimic complex structures, such as capillary vessels, thus incorporating a very important characteristic of solid tumors: angiogenesis [81, 84]. However, this technique requires specific equipment and it is associated with higher costs. Additionally, the underlying disadvantages of scaffold-based approaches mentioned above apply to the structures in which the scaffold is maintained.

2.5.4 Tumor-on-a-chip

While the former models are able to recapitulate several characteristics of the tumor and the TME, there is an important aspect that is lacking: fluid dynamics [85].

Organ-on-chips comprise microfluidic devices in which cells are placed in compartments connected by perfused hollow channels. Therefore, tumor-on-chips are organ-on-chips that incorporate tumor cells [29]. This model enables the crosstalk between different cell types in spatial and temporal controlled conditions in terms of chemical gradients and biological forces [64]. In fact, the fluid flow profile in these devices is mainly laminar, which is characterized by a more predictable and controlled behavior. Hence, the study of several parameters, such as angiogenesis, metastasis, cell behavior, intravasation, extravasation, along with drug response under shear stress is possible [81, 84]. Accordingly, the use of this technique has been reported in breast cancer studies, including to evaluate the behavior, in terms of migration capacity, of non-malignant (MCF-10A) and malignant (MCF-7 and MDA-MB-231) breast cancer cell lines [59]. Downsides of these systems comprise their high complexity, as well as the requirement of specific equipment, just like in 3D bioprinting [29].

In summary, different 3D models display distinctive characteristics that make them suitable for studying tumorigenesis, as well as for drug screening purposes. While the more advanced models, such as tumor-on-a-chip and 3D bioprinting, are able to recapitulate a wider spectrum of conditions associated with *in vivo* tumors, they rather often incorporate organoids and spheroids in their systems. Consequently, the establishment and characterization of a simplistic, yet robust model that can be later integrated into more complex systems is crucial to encourage the development of more relevant studies on breast cancer biology, as well as to further improve the feasibility of the results regarding drug screening studies.

Chapter 3

Materials and Methods

3.1 Ethics statement

Human blood samples were obtained according to the ethical principles stated in the Declaration of Helsinki. Monocytes were isolated from buffy coats of healthy blood donors, kindly provided by the Immunohemotherapy Department of Centro Hospitalar de São João (CHSJ), Porto, Portugal. Informed written consent was given by the blood donors on the utilization of their blood collection byproducts for research purposes. All the procedures were approved by the CHSJ Ethics Committee (protocol 90/19).

3.2 Human monocyte isolation

Monocytes were isolated from buffy coats of healthy blood donors, as previously optimized by others [93]. Briefly, the procedure initiated with the centrifugation of the blood samples, in order to collect the peripheral blood mononuclear cells (PBMCs), to which was then added RosetteSep^{TM} Human Monocyte Enrichment Cocktail (StemCell Technologies). This reagent allows the isolation of monocytes through a process of negative selection, in which undesired (non-monocyte) cells are crosslinked to red blood cells (RBCs) by tetrameric antibody complexes (TACs), resulting in the formation of dense immunorosettes [94]. Afterwards, the rosettes were added to Ficoll-Histopaque (Sigma-Aldrich), a buoyant density medium, and the mixture was centrifuged. During centrifugation, a gradient was formed: the rosettes, which are denser, pelleted beneath the Ficoll-Histopaque, while the monocytes were placed between the density medium and the plasma. Finally, monocytes were collected and washed 3 times with PBS before being resuspended in Roswell Park Memorial Institute (RPMI) 1640 medium (Gibco®), supplemented with 10% of heat inactivated fetal bovine serum (FBS, Biowest) and 1% of penicillin-streptomycin (Pen-Strep) solution.

3.3 Cell culture

The MCF-7 human breast cancer cell line, provided by Dr. Meriem Lamghari (i3S, Porto, Portugal), was cultured in Dulbecco's Modified Eagle Medium/Nutrient Mixture F-12 (DMEM/F-12, Gibco®), supplemented with 10% (v/v) of heat-inactivated FBS (Biochrom GmbH) and 1% (v/v) of Pen-Strep solution. Human mammary fibroblasts (hMFs) were kindly provided by Dr. Sílvia Bidarra (i3S, Porto, Portugal). These cells were cultured in DMEM with ultraglutamine-1 (Lonza), supplemented in the same conditions mentioned above. All cells were handled under aseptic conditions, and incubated at 37 °C in a 5% CO_2 atmosphere.

3.4 Multicellular tumor spheroid assembly

To establish MCTS, the liquid overlay technique (LOT), using agarose as a non-adhesive surface, was the method used. As such, commercially available micro-molds (3D Petri Dish®, by MicroTissues, Inc.), with 81 circular recesses distributed in a 9x9 array, were used to make agarose molds, on top of which cells were seeded. Briefly, 0.9% (w/v) of sterile sodium chloride (NaCl) solution was added to a sterile agarose powder and dissolved to form a solution of 2% (w/v) agarose (SeaKEM® LE Agarose, Lonza). Then, the agarose solution was casted and allowed to solidify in the micro-molds to form the agarose molds, which were later transferred to sterile 12-well plates. To equilibrate the molds, they were later incubated with complete culture medium (1.5 mL) for at least 2 h. Afterwards, the medium was removed and cells were collected and counted in order to prepare the adequate cell suspensions, according to the total number of cells per spheroid. Finally, 190 μL of each cell suspension were seeded onto the corresponding mold and the plate was left still for approximately 30 min at room temperature (RT), so as to enable cells to settle inside the molds. After the incubation time, 2 mL of medium was added to each well and cells were incubated at 37 °C in a 5% CO_2 atmosphere. The medium of the spheroids was changed every two days.

The studies firstly began with the development of a monoculture spheroid model, containing exclusively MCF-7 cells. After the characterization of this model, a double culture spheroid model, combining MCF-7 cells and hMFs, was produced and characterized. Finally, monocytes were added to the previous model to form triple culture spheroids, which ultimately represent the 3D platform to be used for drug screening. Different cellular concentrations and cellular ratios of each cell type were tested.

3.5 Multicellular tumor spheroid characterization

Several assays were performed to characterize the 3D models developed, namely the measurement of the MCTS size, the resazurin assay to evaluate the metabolic activity, histological analysis by hematoxylin and eosin staining, immunohistochemistry, flow cytometry analysis and live/dead assay.

3.5.1 Size measurement

Brightfield images of the spheroids produced were taken at three specific timepoints – days 1, 4 and 7 after cell seeding –, using ZOE™ Fluorescent Cell Imager (Bio-Rad Laboratories). The size was determined by measuring the diameter of the MCTS through the ImageJ software. The diameter of the MCTS was determined by manually performing two measurements in per spheroid, and subsequently calculating the average of the two values obtained. At each condition, 5 different MCTS were measured.

3.5.2 Metabolic activity

The MCTS metabolic activity was measured through the resazurin assay. Briefly, at days 1, 4 and 7 after cell seeding, the medium was removed from each mold and 2 mL of culture media containing 20% of resazurin (v/v) were added to each well. Afterwards, the spheroids were incubated for 2 h at 37°C in the dark. Following the incubation period, 200 μL of medium from each condition was transferred to a black-walled, clear-bottom 96-well plate (Corning Costar®), in triplicates. Finally, the fluorescence was measured at the excitation and emission wavelengths of 530 nm and 590 nm, respectively, using SynergyMx™ MultiMode Microplate Reader (BioTek™).

3.5.3 Live/dead cell assay

Additionally, a viability assay was performed to assess the formation, over time, of a necrotic core in the MCTS, using LIVE/DEAD™ Viability/Cytotoxicity Kit (Invitrogen), constituted by calcein AM and ethidium homodimer-1. These reagents allow the imaging of live and dead cells, respectively. The protocol consisted in washing the molds three times with PBS, after which cells were incubated with calcein AM (0.5 µL/mL in PBS) and ethidium homodimer-1 (2 µL/mL in PBS) for 30 min at RT (200 µL). After this period of incubation, cells were, once more, washed three times with PBS. Imaging of the live/dead-labelled spheroids was accomplished using fluorescence widefield HCS microscope IN Cell Analyzer 2000 (GE Healthcare). All acquired data was processed using IN Cell Developer Toolbox and ImageJ software.

3.5.4 Histological analysis

At the same pre-determined timepoints, the media was removed from the wells and the molds were washed twice with PBS (2 mL), after which the spheroids were fixed in a solution of 4% (v/v) PFA (DeltaMicroscopes) in PBS. Specifically, 2 mL of PFA 4% was added to the wells and the molds were left incubating for 30 min at RT. The PFA was later removed from the molds and they were once again washed twice with PBS. Then, 200 µL of 1% agarose (w/v) solution was added to the top of the molds. The agarose was allowed to solidify and, afterwards, the samples were put in cassettes, which were then placed in a PBS 1x solution. Subsequently, the samples were processed, embedded in paraffin, sectioned and finally deparaffinized in xylene and rehydrated in a gradually decreasing ethanol series. Finally, staining with hematoxylin and eosin (H&E) was performed to each section.

3.5.5 Immunohistochemistry

Immunohistochemistry staining was performed, at day 7 after cell seeding, as described elsewhere [95]. Firstly, samples, which were fixed according to the protocol described above, were sectioned and deparaffinized in xylene, followed by rehydration in a gradually decreasing series of alcohol concentrations. Afterwards, sections were incubated with the respective antigen retrieval buffers – sodium citrate buffer (10×10^{-3} M; pH=6) or Tris-EDTA buffer (10×10^{-3} M Tris, 1×10^{-3} M EDTA; pH=9) for 30 min, at 96 °C. Following this incubation period, sections were washed three times with PBS for 5 min, under agitation (60 rpm). Next, samples were permeabilized by immersing the sections in Triton X-100 0.25% (v/v in PBS), for 30 min at 60 rpm, and were again washed three times with PBS, as stated above. Then, samples were blocked with 10% (v/v) of FBS in PBS for 1 h at RT. After that time, the primary antibodies (Table 1) were diluted in a solution of 5% (v/v) FBS in PBS, added to the corresponding sections and allowed to incubate overnight, in a wet chamber, at 4 °C. Samples were then washed three times with PBS in the former conditions. The secondary antibodies (Table 2) and DAPI solution were diluted in 5% (v/v) of FBS in PBST, added to the respective sections and left incubating in the dark, in a wet chamber, for 1 h at RT. Lastly, sections were mounted with Fluorescence Mounting Medium

(Dako) and imaged using Zeiss AxioImager Z1 microscope (Carl Zeiss), equipped with an AxioCam MR ver.3.0.

Table 1 Information on the primary antibodies used for immunohistochemistry analysis.

Targeted Antigen	Species Source	Manufacturer	Antibody dilution	Retrieval buffer
ZO-1	Rabbit	SantaCruz Biotechnologies	1:40	Sodium citrate buffer
Vimentin (v9)	Mouse	SantaCruz Biotechnologies	1:50	Sodium citrate buffer
CD68	Mouse	Dako	1:100	Tris-EDTA buffer
Fibronectin	Rabbit	Sigma	1:200	Sodium citrate buffer

Table 2 Information on the secondary antibodies and DAPI solution used for immunohistochemistry analysis.

Antibody	Manufacturer	Antibody dilution	Anti	Produced in
Alexa Fluor 488 Ig	Invitrogen	1:400	Rabbit	Goat
Alexa Fluor 594 F(ab')2 fragment of IgG (H+L)	Invitrogen	1:400	Mouse	Goat
DAPI	Merck Millipore	1:2 (aliquots at 1 µg/mL)		

3.5.6 Flow cytometry

Flow cytometry was later performed to further characterize the triple co-culture spheroids at days 1, 4 and 7 after cell seeding, as described elsewhere [95]. Briefly, at each timepoint, approximately 40 MCTS per mold were collected into a 15 mL falcon tube and centrifuged at 1200 rpm for 5 min, at 4°C. Following centrifugation, the medium was removed and cells were washed once with PBS (2 mL) by centrifugation, in the same conditions. After the removal of the supernatant, the spheroids were dissociated to a single cell suspension by adding 300 µL of trypsin and incubating for 30 min at 37 °C. During the incubation time, MCTS were mechanically dissociated by pipetting the suspension every 5 min. Then, complete media (2 mL) was added to the tube to inactivate trypsin and cells were washed with FACS buffer (2mL) (PBS containing 2% and 0.01% sodium azide) and transferred to a non-coated round bottom 96-well plate (Corning Costar®). Cells were then centrifuged (1500 rpm, 5 min, 4 °C), resuspended in 50 µL of a solution of FACS buffer with the antibodies (FITC-anti-E-cadherin 1:200 (BioLegend), PerCP-Cy5.5-anti-CD90 1:100 (BD Biosciences) and APC-anti-CD14 1:25(ImmunoTools)) and incubated in the dark for 30 min at 4 °C. After incubation, cells were washed twice with PBS containing 2% FBS (1500 rpm, 5 min, 4 °C) and resuspended in 100 µL of a live/dead solution (1:10000) (eBioscience™ Fixable Viability Dye eFluor™). Finally, samples were washed were washed as previously, and fixed in a solution of PFA 1% (v/v). To analyze the samples, they were filtered through a 70 µm pore filter membrane. The equipment used for the analysis was the BD

FACSCanto^{TM} II flow cytometer (BD Biosciences) and all the acquired data was processed using FlowJo software.

3.6 Production of gefitinib-encapsulated PLGA nanoparticles

The poly (lactic co-glycolic acid) (PLGA) nanoparticles (NPs) were prepared by a nanoprecipitation technique, as described elsewhere [96]. Both non-loaded NPs and NPs loaded with GEF were produced. Firstly, the organic phase was prepared by weighting 16 mg of PLGA (Corbion), 4 mg of PLGA-PEG-Maleimide (Ruixibiotech) and 1.1 mg of GEF (5% drug loading) (SantaCruz Biotechnology) into a tube and dissolving this mixture in 3 mL of dimethylformamide (AcrosOrganics). In case of the empty NPs, only 16 mg of PLGA and 4 mg of PLGA-PEG-Mel were weighted. The tubes solution containing the organic phase were left at RT overnight covered with parafilm to avoid organic solvent evaporation. In the following day, the aqueous phase, which consisted in 10 mL of 1% of Tween 80 (Sigma Aldrich) in MilliQ® ultrapure water (pH=7.4), was prepared. Afterwards, NPs were produced by injecting the organic phase into the aqueous phase with a 25G needle. The solution was then left under magnetic stirring (200 rpm), for 3 h at RT. To remove the surfactant of the aqueous phase and the non-encapsulated drug, the obtained colloidal was washed three times with MilliQ® ultrapure water and recovered by ultracentrifugation (600 g x for 10 min; 4 °C; Eppendorf Centrifuge 5804R) using Amicon® centrifugal filter units with a weight molecular cut-off (MWCO) of 100 kDa.

3.7 Characterization of the nanoparticles

Both NP formulations were characterized for their average size and polydispersity index (PdI) by dynamic light scattering (DLS), and zeta-potential through laser Doppler anemometry (LDA), using a Malvern Zetasizer Nano ZS equipment (Malvern Instruments Ltd). To prepare the samples for analysis, NPs were diluted (1:100) in a solution of 10 mM NaCl, at pH=7.4. For each formulation, three measurements were registered. The final values are represented as the following: mean ± standard deviation.

3.8 Evaluation of gefitinib nanoparticles therapeutic efficacy in the established breast cancer 3D model

Triple co-culture MCTS were cultured for 7 days in RPMI 1640 complete medium, as previously described. At day 7, the spheroids were transferred from the molds into non-coated round-bottom 96-well plates (Corning Costar®) (1 spheroid per well) and 100 µL of different treatments were added to the cells: empty NPs, gefitinib loaded-NPs or free gefitinib. For each therapeutic approach, three concentrations were tested: 100 µg/mL, 500 µg/mL and 1000 µg/mL, comprising a total number of nine conditions. Spheroids were left incubating with these suspensions for 24 h and 48 h, at 37 °C in a 5% CO_2 atmosphere. Triplicates were considered for each condition. At these specific timepoints, different assays were performed to assess the therapeutical effect of the nanoparticles in the 3D model developed, including the live/dead assay, resazurin assay and CellTiter-Glo® 3D viability assay. Untreated spheroids were used as control.

3.8.1 Assessment of the nanotherapeutic effect in cell viability

After 24 h of treatment, a live/dead assay was performed to assess whether NPs could affect cell viability. The protocol was similar to the one applied for the MCTS characterization, though with slight modifications: the medium was removed from the wells, and spheroids were incubated with 50 μL of a solution of calcein AM/ethidium homodimer-1 in PBS, prepared in the previous concentrations, for 30 min at RT. Afterwards, spheroids were washed once with PBS and visualized in a fluorescence widefield HCS microscope IN Cell Analyzer 2000 (GE Healthcare).

Further, this evaluation was complemented with the measurement of ATP levels through a specific kit for 3D cell models. CellTiter-Glo® 3D Cell Viability assay (Promega Corporation) was performed 48 h after starting the treatment. The CellTiterGlo® 3D reagent measures the amount of ATP present, which acts as an indicator of the number of viable cells in culture. The protocol consisted in adding an equal amount of reagent to the volume of medium in the wells (100 μL) and shaking the plates for 5 min at 100 rpm, after which cells were incubated at RT for 25 min. The solution contained in each well was transferred to a white, opaque 96-well plate (Sterilin Limited) and luminescence was detected (integration time: 0.8 seconds per well) using SynergyMx™ MultiMode Microplate Reader (BioTek™).

3.8.2 Assessment of the nanotherapeutic effect in metabolic activity

The metabolic activity of the spheroids was, once more, evaluated through the resazurin assay, 24 h and 48 h after treatment initiation. Therefore, at these timepoints, the medium was removed and 150 μL of resazurin 10% (v/v) in complete medium were added to each well. Following 2 h of incubation at 37 °C, 100 μL of medium from each well were removed and put into clear-bottom black 96-well plates (Corning Costar®). The fluorescence was measured as mentioned above.

3.9 Nanotherapeutic treatment in MCF-7 2D cell culture

Aside from evaluating the effect of gefitinib-encapsulated NPs in the spheroid model developed, the outcomes of this treatment were also monitored in MCF-7 cells, cultured in 2D. Therefore, MCF-7 cells were counted, seeded in a sterile 96-well plate (1×10^4 cells per well) and incubated overnight to enable their attachment. In the following day, the medium was removed and cells were treated in an identical way to the MCTS: three different treatments were tested at three different concentrations, considering 100 μL of complete medium as a negative control as well. Triplicates were equally planned for each condition. Similar to the 3D culture, live/dead assay was performed at 24 h after treatment, while the resazurin assay was carried out 24 h and 48 h upon treatment initiation.

Chapter 4

Results and Discussion

4.1 Development and characterization of a monoculture breast tumor spheroid model

To achieve the ultimate goal of this dissertation – that is, the development of a 3D triple culture MCTS model to be used as a platform for drug screening –, monoculture MCTS were primarily established and characterized. Therefore, the model firstly comprised solely breast cancer cells, which was then followed by the progressive addition of fibroblasts and monocytes, respectively, in order to understand the influence of each cell type in the overall MCTS structure and metabolic activity.

As previously stated, luminal A breast cancer is the most common molecular breast cancer subtype. Therefore, the MCF-7 cell line, a luminal A poorly-invasive breast cancer cell line, was chosen for the development of this model, as it constitutes a broader representation of this disease [97]. Nevertheless, it is important to mention that MCF-7 cells cannot fully recapitulate breast cancer heterogeneity. Hence, the implementation of MCTS models with different breast cancer lines would promote a better characterization of this disease.

For the development of MCF-7 monoculture spheroids, MCF-7 cells were seeded on top of agarose molds, as formerly described. Four different cellular concentrations (1,000, 2,500, 5,000 and 10,000 cells per spheroid) were tested and cultured for seven days in DMEM/F12 culture medium. Throughout that time, the metabolic activity, as well as the size and morphology of the spheroids were assessed at three specific timepoints: 1, 4 and 7 days after seeding the cells (Figure 5).

Regarding the morphology of the spheroids, these cells formed compact structures within one day (D1) of culture (Figure 5A), maintaining that morphology for, at least, seven days. Moreover, the diameter of the MCTS was apparently conserved throughout the days (Figure 5B). These results are consistent with growth patterns previously reported in some of these 3D structures, which detailed an exponential growth in spheroids with less than 200 μm in diameter, followed by a slower growth rate that ultimately culminated in a growth plateau [98]. The size evaluation also indicates that the MCTS diameter seems to be dependent on the cell seeding concentration throughout the 7 days of culture.

The metabolic activity, on the other hand, registered a high variability between experiments with no evident alterations overtime. (Figure 5C). Considering the nearly constant size observed in most conditions, it would be expected that the metabolic activity levels would be approximately maintained overtime. Yet, it is important to note that, in larger MCTS, the cells in the innermost layer get deprived of nutrients, which likely affects both their growth kinetics and metabolic activity. Nevertheless, regarding this issue, the results obtained were not conclusive, so further experiments should be performed. Further, this colorimetric assay may not be the most suitable for evaluating cell viability, as the dye may not homogeneously infiltrate the structure, which can influence the accuracy of the results [98].

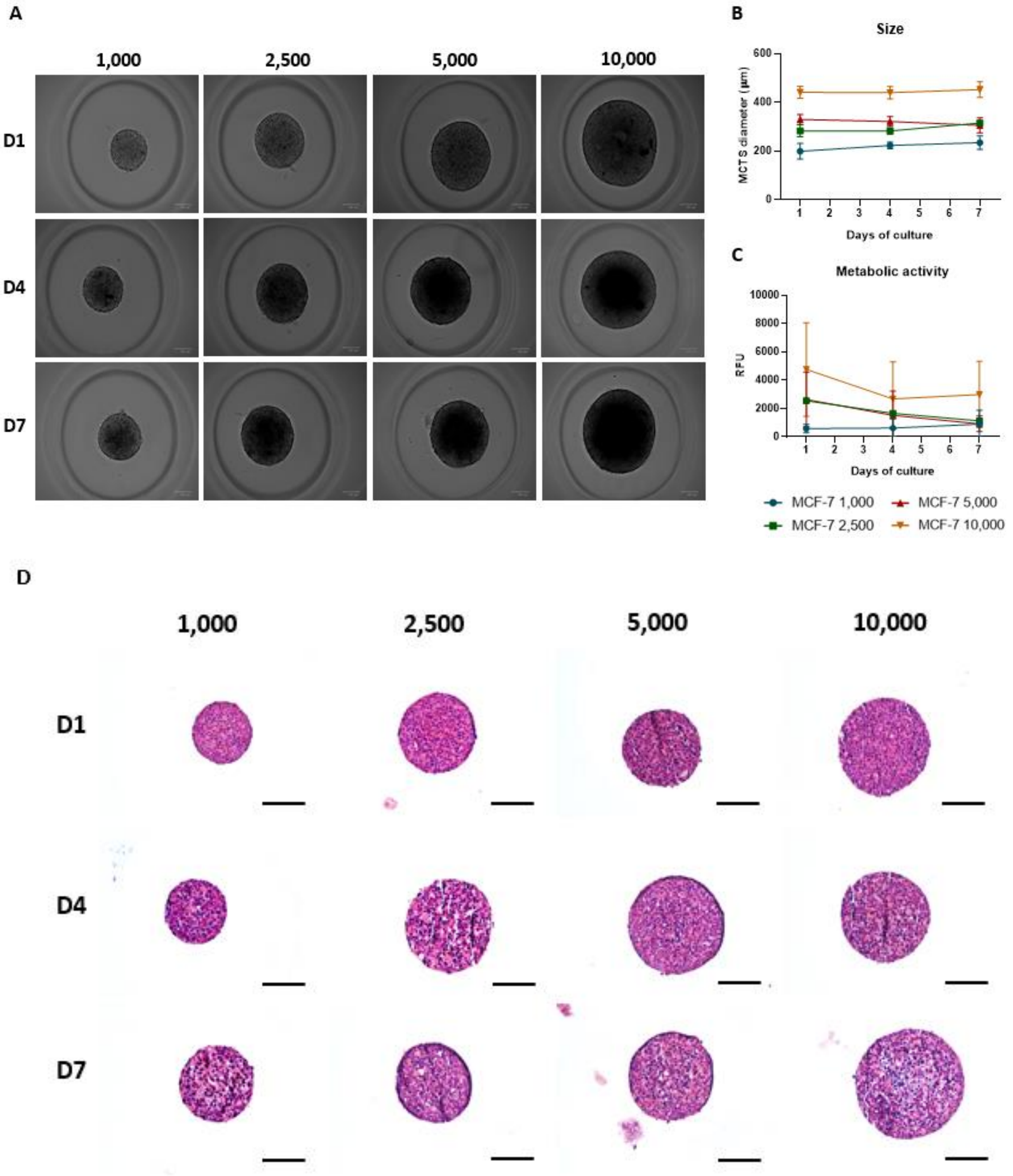
A
1,000
2,500
5,000
10,000
D1
D4
D7
B
Size
MCTS diameter (µm)
600
400
200
0
1
2
3
4
5
6
7
Days of culture
C
Metabolic activity
RFU
10000
8000
6000
4000
2000
0
1
2
3
4
5
6
7
Days of culture
MCF-7 1,000
MCF-7 5,000
MCF-7 2,500
MCF-7 10,000
D
1,000
2,500
5,000
10,000
D1
D4
D7

Figure 5 Characterization of MCF-7 monoculture MCTS, assembled at four different initial cell densities, over seven days of culture. **A)** Brightfield microscopy images of the MCTS morphology, taken at days 1, 4 and 7 after cell seeding. Scale bars represent 100 µm. **B)** Measurement of the MCTS diameter from the brightfield images taken. Values represent mean ± SD (n=5 spheroids analyzed per condition, 2 independent experiments). **C)** Evaluation of the MCTS metabolic activity at the formerly mentioned timepoints, according to the initial cell density. Values represent mean ± SD (n=81 spheroids per condition, 2 independent experiments). RFU: relative fluorescence units. **D)** Histological analysis by H&E staining of the MCTS overtime. Scale bars represent 100 µm.

Finally, the MCTS characterization by H&E staining (Figure 5D) suggested that, after 7 days of culture, these spheroids did not generally develop a distinguished necrotic core in the center of the structure. The larger spheroids represent the only condition in which a necrotic core apparently starts to be developed at the 7th day of culture. Accordingly, it has been reported that, in spheroids with > 400-500 μm in diameter, gradients of O_2 and nutrients are generated over time due to limitations in their diffusion to the center of the 3D structures [29, 99]. The formation of a necrotic structure in spheroids can be characterized by H&E staining through the evaluation of a specific set of morphological features, such as nuclear condensation and fragmentation, reduced cell density and cell rounding [100, 101]. A possibility could be to extend the time of MCTS culture, in order to mimic tumor spheroids in more advanced stages of the disease.

Following this characterization, no evident differences were observed between the tested concentrations. Hence, it was decided to narrow the number of conditions in order to pursue the upcoming studies. Therefore, the establishment of double culture spheroids was carried out considering two initial cell densities: 2,500 cells and 5,000 cells/spheroid.

4.2 Development and characterization of a double co-culture breast tumor spheroid model

After the characterization of the monoculture spheroids, a double culture MCTS model was established by adding normal human mammary fibroblasts (hMFs), one of the major components of the breast TME [56]. For each of the cell seeding concentrations considered for this study, two cellular ratios of MCF-7 cells to hMFs were tested – 1:1 and 1:3. The latter ratio mimics breast tumors in more advanced stages, which are characterized by a greater stromal content in comparison to breast cancer cells [102]. Moreover, MCF-7 cells and hMFs were individually cultured as control conditions. Similar to the monoculture spheroids, double co-culture MCTS, seeded at 2,500 cells/spheroid (Appendix A) or 5,000 cells/spheroid (Figure 6), were maintained for 7 days and the same assays were performed at the previously determined timepoints: 1st, 4th and 7th days of culture.

The morphological analysis of the co-culture MCTS revealed that, regardless of the initial cell density or the cellular ratio of MCF-7 cells to hMFs, compact structures were formed one day after seeding the cells (Figure 6A). Interestingly, in all the co-culture conditions tested, the diameter of the spheroids apparently increased throughout the days (Figure 6B), as opposed to what was observed in the monoculture spheroids produced (Figure 5B). Furthermore, the metabolic activity followed a similar trend, with the double culture spheroids seemingly showing an increase when compared to the monoculture conditions (Figure 6C). Therefore, these results apparently indicate that the addition of fibroblasts to MCF-7 cells induces a shift in the MCTS growth kinetics, as well as in the metabolic activity, which is corroborated by the fact that fibroblasts secrete cytokines, exosomes and growth factors (namely TGF-β, growth differentiation factor 15, leukaemia inhibitory factor, etc.) that can promote a more invasive and proliferative behavior in cancer cells [103]. Nevertheless, more studies would need to be carried out in order to statistically validate these results.

Results further suggest that the two cellular ratios (1:1 and 1:3, MCF-7:hMF) do not display perceptible differences in the size or metabolic activity of the MCTS (Figure 6C). On the one hand, considering the higher proliferation rate of tumor cells, it could be expected that the conditions comprising a higher MCF-7 cell ratio (1:1) would display a higher growth rate, as well as higher levels of metabolic activity. On the other hand, however, the 1:3 (MCF-7:hMF) condition comprises a higher number of fibroblasts, which are known to enhance tumor cells proliferation, as previously stated. As little is still known about the influence of the crosstalk between these two cell types in 3D structures, more studies should be performed to fully elucidate the effects of this interaction.

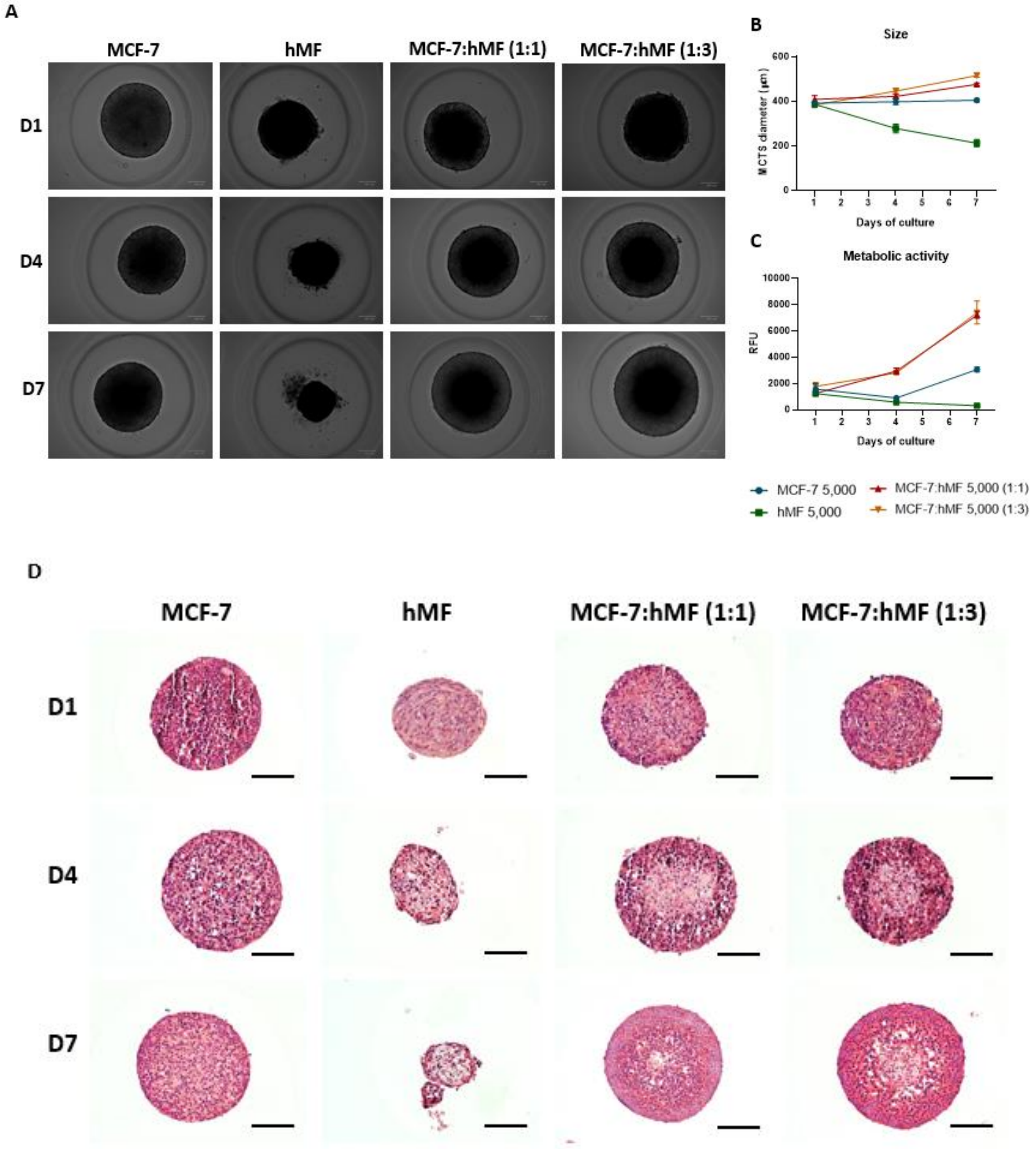
A
MCF-7
hMF
MCF-7:hMF (1:1)
MCF-7:hMF (1:3)
D1
D4
D7
B
Size
MCTS diameter (µm)
0
200
400
600
1
2
3
4
5
6
7
Days of culture
C
Metabolic activity
RFU
0
2000
4000
6000
8000
10000
1
2
3
4
5
6
7
Days of culture
MCF-7 5,000
hMF 5,000
MCF-7:hMF 5,000 (1:1)
MCF-7:hMF 5,000 (1:3)
D
MCF-7
hMF
MCF-7:hMF (1:1)
MCF-7:hMF (1:3)
D1
D4
D7

Figure 6 Characterization of MCF-7:hMF double co-culture MCTS, assembled at the initial cell density of 5,000 cells/spheroid, over seven days of culture. Two cellular ratios of MCF-7 cells to hMFs were tested – 1:1 and 1:3. MCF-7 and hMF monoculture MCTS were cultured as control spheroids. **A)** Brightfield microscopy images of the MCTS morphology, taken at days 1, 4 and 7 after cell seeding. Scale bars represent 100 µm. **B)** Measurement of the MCTS diameter from the brightfield images taken. Values represent mean ± SD (n = 5 spheroids per condition, 1 independent experiment). **C)** Evaluation of the MCTS metabolic activity at the formerly mentioned timepoints, according to the initial cell density. Values represent mean ± SD (n=81 spheroids per condition, 1 independent experiment). RFU: relative fluorescence units. **D)** Histological analysis by H&E staining of the MCTS overtime. Scale bars represent 100 µm.

Regarding the histological analysis of these structures, nuclear disintegration was visible in the double culture spheroids at later stages of culture, particularly at the 1:3 cell ratio (Figure 6D). Finally, the immunostaining performed in double culture spheroids with an initial number of 5,000 cells per spheroid enabled a better understanding of the spatial organization of these two cell types within the MCTS produced (Appendix B). Therefore, hMFs (which stain positive for vimentin) were mainly localized at the center of the spheroid, supporting the H&E

characterization that suggested a reorganization of these cells to the core of the spheroid at day 4. These results are coherent with similar studies in which co-culture spheroids were formed by simultaneously seeding fibroblasts and breast cancer cells [104]. However, this cellular organization does not recapitulate the clinical situation, in which fibroblasts are more uniformly distributed within the breast tumor [105]. As such, a recent study has evaluated the impact of a different cell seeding approach in the breast MCTS morphology, in which breast cancer cells and fibroblasts were sequentially seeded within a 24 h break [104]. The spheroids displayed a more uniform fibroblast distribution, which may constitute a more clinically relevant model. Hence, it could be interesting to further optimize this model by testing the impact of different cell seeding approaches in the cellular organization of these spheroids.

Apparently, there was no prominent variation among the results obtained concerning the two seeding concentrations (Appendix A and Figure 6). Consequently, the following studies were pursued with the highest initial cell density (5,000 cells/spheroid). The reason for this choice is related to the fact that the final model aims at working as a platform for drug screening, thus being important for it to have a considerable number of cells in order to more appropriately predict the effect that drugs will have on the tumor. Furthermore, the cellular ratio of 1:1 (MCF-7:hMF) was chosen.

Importantly, the fibroblasts used in this study were originated from healthy mammary tissue. Therefore, they may not display the same characteristics of CAFs. However, previous studies have shown that healthy fibroblasts co-cultured with MCF-7 cells in a 3D MCTS structure expressed high levels of α-SMA after 7 days of culture, which is a frequently used marker to indicate the presence of CAFs [104]. Moreover, breast cancer cells also promote the differentiation of cells into a CAF-like phenotype, through the secretion of growth factors, such as TGF-β1, or through the Notch signaling, as previously reported [58, 103]. Nevertheless, it could be interesting to evaluate the levels of TGF-β on culture medium of MCTS as well as the activation of its receptors on hMFs.

4.3 Development and characterization of a triple co-culture breast cancer spheroid model

Following the characterization of the monoculture and double culture MCTS, the model was further improved to better mimic the tumor’s complexity by seeding monocytes isolated from buffy coats of healthy blood donors simultaneously with fibroblasts and MCF-7 cells. In this experiment, the culture medium was changed to RPMI, since monocytes culture was previously established in this medium [93] and it is expected to add T cells to the model in future studies, which are usually cultured in RPMI 1640 medium [106]. Therefore, MCF-7 spheroids were cultured in DMEM/F12 and in RPMI, in order to evaluate the differences regarding their metabolic activity and size (Appendix C). The results suggest that MCF-7 cells are more proliferative in RPMI culture medium. Accordingly, studies from colleagues have recently shown that culture medium displays a significant impact on several aspects of the cells, such as metabolic activity, ATP generation, immune interactions and also radiotherapy response (Arne Peirsman *et al., Nature methods*, accepted). These data reinforce the importance of the selection of the media type when designing studies using spheroids, inclusively when the aim is to investigate the effects of therapeutic intervention.

For the development of this model, the cell seeding concentration, as well as the cellular ratio of MCF-7 cells to hMFs were fixed at 5,000 cells/spheroid and 1:1 (MCF-7:hMF), respectively, as stated above. Yet, different cell ratios of monocytes to the remaining cell types were tested – (MCF-7:monocytes:hMFs) – 1:2:1, 1:4:1 and 1:10:1. The conditions used as control included the individual seeding of MCF-7 cells, as well as co-culture MCTS comprising MCF-7 cells and monocytes, at three cellular ratios – 1:2, 1:4 and 1:10 of MCF-7 cells to monocytes. As previously executed, MCTS were maintained in culture for 7 days and the characterization of these structures was performed at the same timepoints as before (Figure 7).

Unlike the monoculture (MCF-7) and double culture (MCF-7:hMF) spheroids, in which very compact structures were formed within one day of culture, the triple culture spheroids showed, within the same period of time, a main compact cellular structure surrounded by a few cell aggregates that were spread throughout the well (Figure 7A). These aggregates most likely corresponded to monocytes that were not able to infiltrate the compact MCTS. As the days passed, however, the spheroids became more compact, with less cell aggregates surrounding them, especially in the condition with the smallest ratio of monocytes – 1:2:1 (MCF-7:monocytes:hMF).

Regarding the size of the spheroids, all conditions showed a tendency to increase the MCTS diameter, as already seen in the double co-culture spheroids (Figure 7B). This increase seems more evident between day 1 and day 4 of culture. Furthermore, these results suggest a correlation between the ratio of monocytes (and remaining cells) and the size of the spheroids: the lower the monocyte ratio (and, therefore, the higher the number of MCF-7 cells and fibroblasts) the greater the diameter of the MCTS. The metabolic activity also seemingly increased overtime, with the triple culture spheroids that contained less monocytes (and more MCF-7 cells) displaying higher metabolic levels than those with more monocytes in their composition (Figure 7C). This was expected since MCF-7 cells have a highly proliferative nature, unlike monocytes.

The histological analysis confirmed the formation of cell aggregates in the surroundings of the spheroids, especially at day 1 after cell seeding (Figure 7D). Moreover, some cell fragmentation in the core of the spheroids was visible at day 7 of culture, indicating the formation of a necrotic core, especially in the conditions with a higher ratio of MCF-7 cells and fibroblasts in relation to the monocytes. These results are consistent with the size evaluation overtime, as the larger spheroids corresponded to the ones with a more prominent necrotic core.

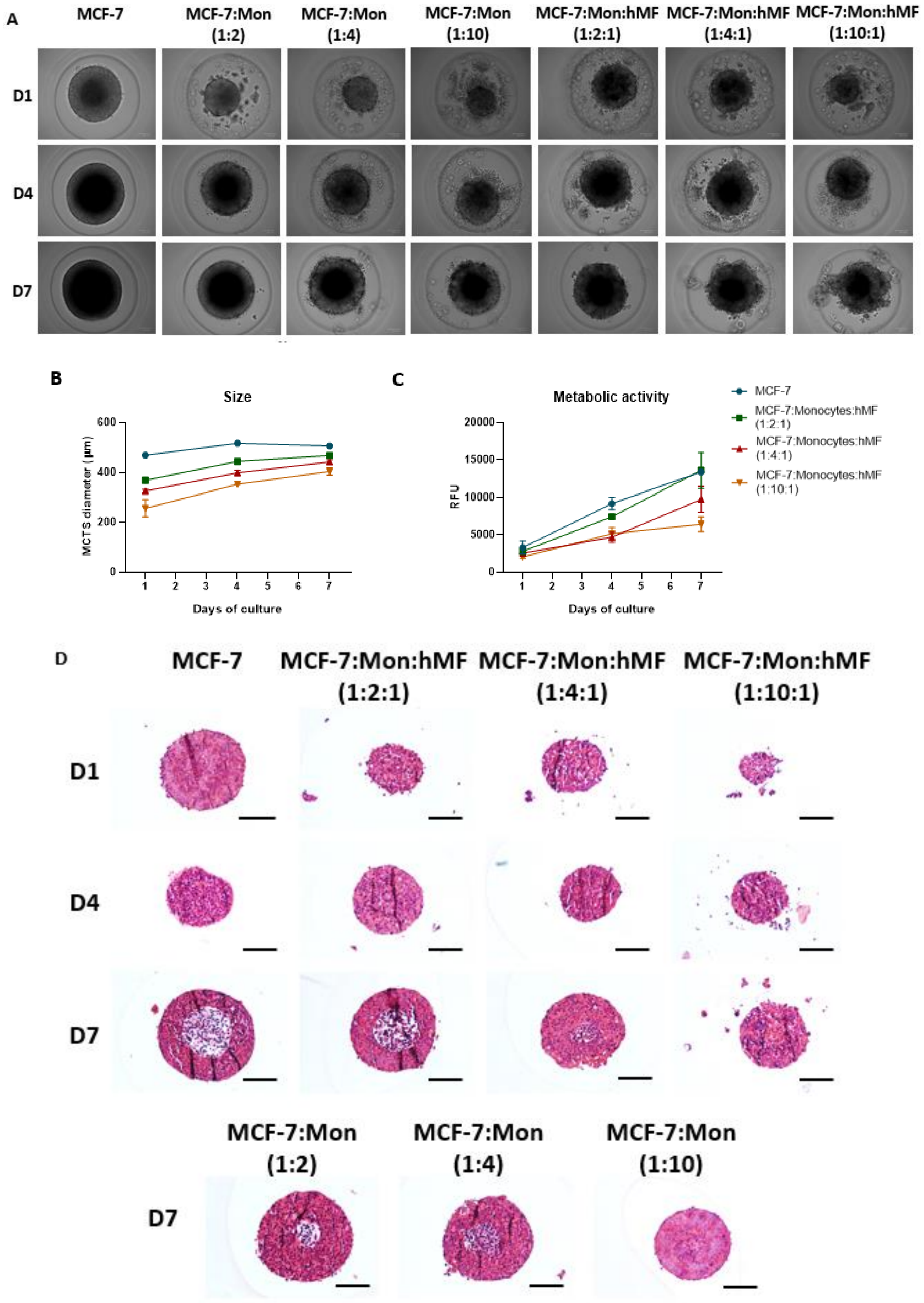
A
MCF-7
MCF-7:Mon (1:2)
MCF-7:Mon (1:4)
MCF-7:Mon (1:10)
MCF-7:Mon:hMF (1:2:1)
MCF-7:Mon:hMF (1:4:1)
MCF-7:Mon:hMF (1:10:1)
D1
D4
D7
B
Size
MCTS diameter (µm)
600
400
200
0
1 2 3 4 5 6 7
Days of culture
C
Metabolic activity
RFU
20000
15000
10000
5000
0
1 2 3 4 5 6 7
Days of culture
MCF-7
MCF-7:Monocytes:hMF (1:2:1)
MCF-7:Monocytes:hMF (1:4:1)
MCF-7:Monocytes:hMF (1:10:1)
D
MCF-7
MCF-7:Mon:hMF (1:2:1)
MCF-7:Mon:hMF (1:4:1)
MCF-7:Mon:hMF (1:10:1)
D1
D4
D7
MCF-7:Mon (1:2)
MCF-7:Mon (1:4)
MCF-7:Mon (1:10)
D7

Figure 7 Characterization of MCF-7:monocytes:hMF triple co-culture MCTS, assembled at the initial cell density of 5,000 cells/spheroid, over seven days of culture. Three cellular ratios of MCF-7 cells to monocytes to hMFs were tested – 1:2:1, 1:4:1 and 1:10:1. Mon: monocytes. Control conditions comprised MCF-7 monoculture MCTS, as well as MCF-7 cells in co-culture with monocytes, at three different cellular ratios – 1:2, 1:4 and 1:10, respectively. **A)** Brightfield microscopy images of the MCTS morphology, taken at days 1, 4 and 7 after cell seeding. Scale bars represent 100 µm. **B)** Measurement of the MCTS diameter from the brightfield images taken. Values represent mean ± SD (n =5 spheroids per condition, 2 independent experiments). **C)** Evaluation of the MCTS metabolic activity at the

formerly mentioned timepoints, according to the initial cell density. Values represent mean ± SD (n=81 spheroids per condition, 2 independent experiments). RFU: relative fluorescence units. **D)** Histological analysis by H&E staining of the MCTS overtime. Scale bars represent 100 µm. **A, D)** Brightfield images and H&E staining images are from a representative blood donor.

4.3.1 Flow cytometry characterization

To further characterize the triple co-culture MCTS in terms of their cellular composition, an analysis by flow cytometry was performed 1 and 7 days after cell seeding (Figure 8). Since the 1:10:1 (MCF-7:monocytes:hMFs) ratio did not form compact structures within 7 days of culture in the MCTS from both blood donors tested, that condition was not considered for this assay. The antibodies used against each cell type were the following: anti-E-cadherin to stain MCF-7 cells, anti-CD90 against hMFs, and anti-CD14 for monocyte staining.

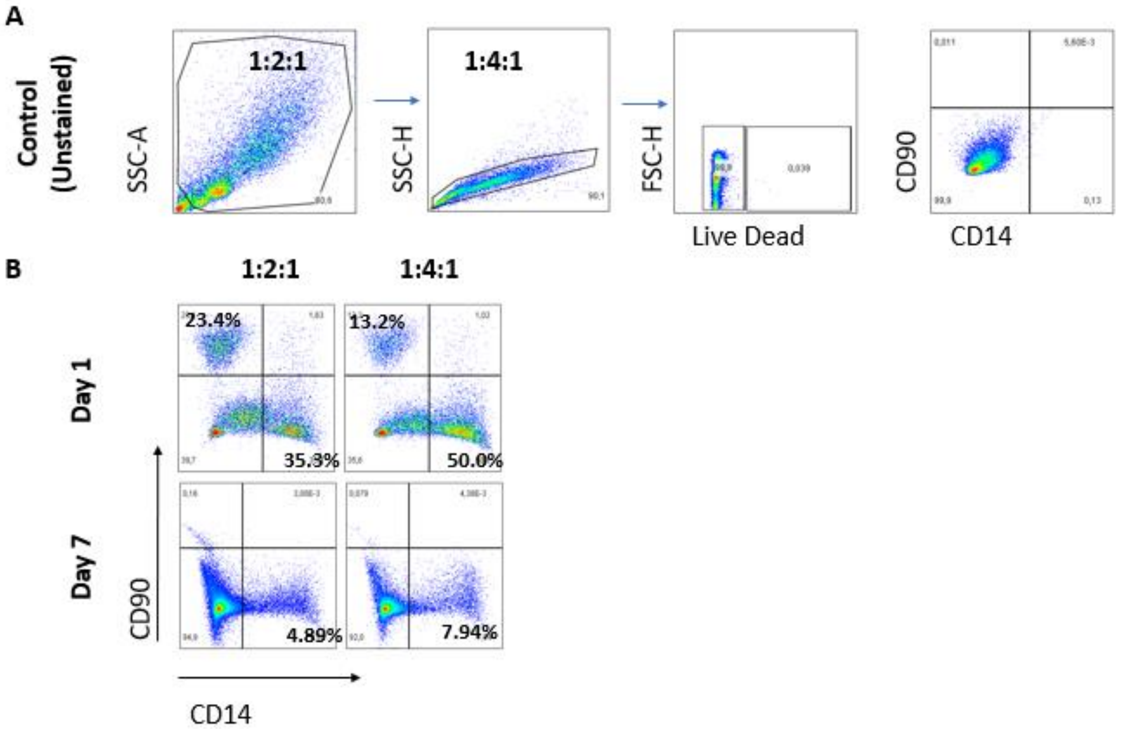

Figure 8 MCF-7 characterization of MCF-7:monocytes:hMF triple co-culture MCTS, assembled at the initial cell density of 5,000 cells/spheroid, by flow cytometry. **A)** Flow cytometry gating strategy to analyze triple co-culture MCTS. Live dead negative cells were gated on single cells. Posteriorly, $CD14^+$, $CD90^+$ and E-cadherin$^+$ cells were gated on live dead negative cells. **B)** Two cellular ratios of MCF-7 cells to monocytes to hMF were tested – 1:2:1 and 1:4:1, at day 1 and day 7 of culture. Numbers indicate the percentage of the previously cited populations.

Looking at the results, MCF-7 cells did not positively stain for E-cadherin, an epithelial cell marker that is part of the adherent junctions (Appendix D). Yet, E-cadherin was expressed in MCF-7 2D cell culture (data not shown). Recent studies have shown that MCF-7 cells lose the expression of E-cadherin when transitioning from a 2D cell culture to an organized 3D spheroid structure [107]. Nonetheless, at day 1, it was possible to extrapolate the percentage of MCF-7 cells present in each structure, since both hMFs and monocytes were positive for the expression markers CD90 and CD14, respectively. However, at day 7, hMFs did not stain for CD90, suggesting that, when incorporated in 3D structures, these cells also lose the expression of this protein overtime (Figure 8B). Regarding the monocytes, there was a considerable decrease in the percentage of these cells between the 1st and 7th days of culture, independently of the cell ratio (Figure 8B). This can be explained by the higher proliferative rate of tumor cells, when compared to non-proliferating monocytes, as well as due to the poor immune infiltration that characterizes luminal A breast cancers [108].

4.3.2 Live/dead assay

Afterwards, a live/dead assay was performed to assess the formation of a necrotic core in the triple culture MCTS model during the 7 days of culture (Figure 9). The viable kit used in this assay contained two dyes: calcein AM and ethidium homodimer-1 (EthD-1) which stain live and dead cells, respectively, based on two important parameters of cell viability: esterase activity and plasma membrane integrity [109]. Quantitative results regarding this assay are shown in Appendix E. Surprisingly, a considerable number of dead cells (EthD-1 positive) were found in the periphery of the spheroids, at day 1 after cell seeding, especially in the co-culture conditions containing monocytes. Theoretically, it would be expected that the majority of the dead cells would be located in the center of the spheroid after a few days of culture, resulting from gradients of oxygenation, pH and nutrients that are likely generated overtime. However, these dead cells were probably not viable at the time of cell seeding, and therefore did not penetrate the MCTS.

Even though the vast majority of the cells remained viable, a few dead cells were visualized over the 7 day-period, likely corresponding to the initial development stage of a necrotic core within the MCTS. A previous study, in which a similar live/dead assay using these dyes was performed in monoculture MCF-7 spheroids, reported that MCTS cell viability was not affected within the first 10 days of culture [110].

It is important to note that the formation of a necrotic core may be desirable, especially for the development of models for drug screening, as tumor necrosis constitutes a feature of solid tumors in more advanced stages [111]. Furthermore, hypoxia and necrosis have been associated with tumor progression and chemoresistance, as the penetration of therapeutic agents is physically and biologically hampered by these conditions [112, 113]. Therefore, it is imperative to recapitulate these hallmarks to obtain feasible results regarding the therapeutic effect of a drug aimed at treating more advanced tumors. Moreover, luminal A breast tumors that resist to endocrine therapy are usually directed to treatment in combination with chemotherapy, which mainly occurs in later stages of the disease. Hence, it could be convenient to maintain the model for different periods of time, in order to recapitulate different stages of cancer.

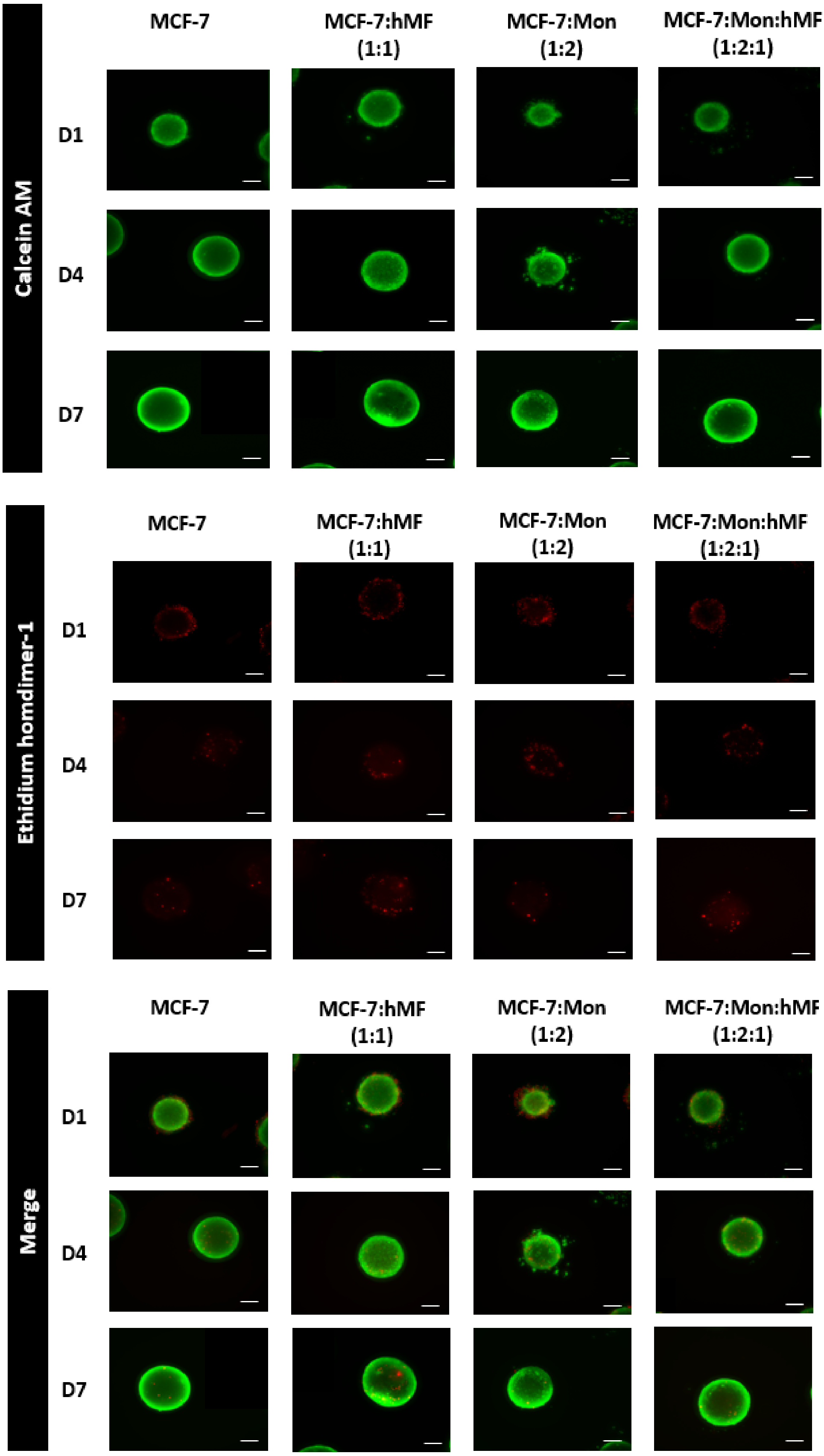
Calcein AM
MCF-7
MCF-7:hMF (1:1)
MCF-7:Mon (1:2)
MCF-7:Mon:hMF (1:2:1)
D1
D4
D7
Ethidium homdimer-1
MCF-7
MCF-7:hMF (1:1)
MCF-7:Mon (1:2)
MCF-7:Mon:hMF (1:2:1)
D1
D4
D7
Merge
MCF-7
MCF-7:hMF (1:1)
MCF-7:Mon (1:2)
MCF-7:Mon:hMF (1:2:1)
D1
D4
D7

Figure 9 Cell viability assessment of the MCTS through a live/dead assay using calcein AM and EthD-1 to stain live and dead cells, respectively. The assay was performed at days 1, 4 and 7 after cell seeding. Green channel: calcein AM; red channel: EthD-1. Scale bars represent 50 µm.

4.3.3 Immunohistochemistry analysis

Finally, immunohistochemistry staining was performed in the monoculture, double culture and triple culture spheroid models developed, fixed at the cell seeding concentration of 5,000 cells per spheroid and the following cellular ratios: 1:1 (MCF-7:hMF) in case of the double culture MCTS model and 1:2:1 (MCF-7:monocytes:hMF) for the triple co-culture MCTS model. This assay was only performed at day 7 of cell culture, which was the final timepoint chosen for the characterization of this model, in order to allow the differentiation of monocytes into macrophages. The immunostaining is shown in Figure 10 and is further detailed in Appendix B.

The antibodies used against each cell type were anti-ZO-1, anti-vimentin and anti-CD68, which stain proteins expressed in MCF-7 cells, hMFs and monocytes/macrophages, respectively. Additionally, the ECM production by the 3D spheroids was assessed by using an antibody against fibronectin, a glycoprotein that is a major component of the ECM [114].

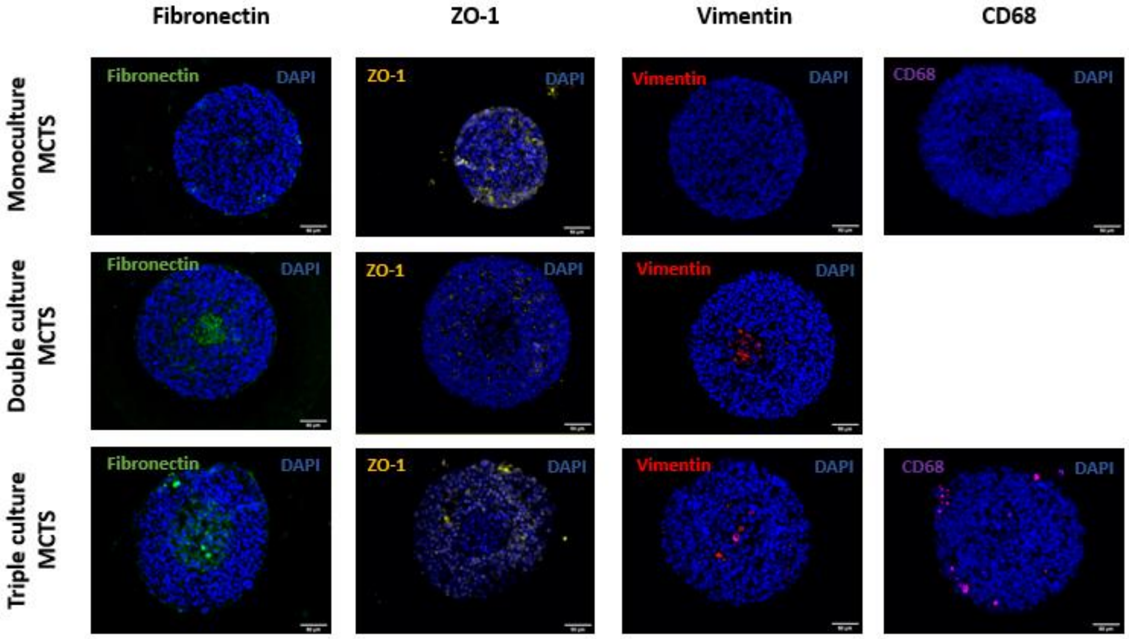

Figure 10 Immunofluorescence microscopy images of mono-, double and triple culture MCTS at day 7 after cell seeding. Fibronectin (green); ZO-1 (yellow); Vimentin (red); CD68 (violet). All samples are counterstained with DAPI (blue channel). Scale bars represent 50 µm.

MCF-7 cells, which have been reported in the literature to express ZO-1 [115], were found mainly in the periphery of the double and triple co-culture spheroids, while the core was mainly populated by vimentin-positive cells, which correspond to the fibroblasts. As mentioned above, this spatial distribution has already been reported in former studies that focused on the development of co-culture spheroids comprising MCF-7 cells and fibroblasts [104].

CD68-expressing cells were mainly located in the border of the triple MCTS, with only a few cells being able to further infiltrate the structure, which is consistent with recently published data concerning the study of monocyte infiltration in MCF-7 breast cancer spheroids [116]. Moreover, luminal A breast cancer subtype was shown to incorporate a significant lower number of macrophages in comparison to the other subtypes, in both the tumor stroma (TS) and the tumor nest (TN) [108].

Lastly, regarding the analysis of the ECM produced by the MCTS, the results suggest that the presence of fibroblasts is associated to fibronectin deposition, as the levels of expression were higher in the center of the co-culture spheroids, where these cells were shown to be mainly located. This was expected since fibroblasts are reported as one of the main cell types that synthesizes fibronectin [114]. On the other hand, MCF-7 cells were shown to produce small amounts of fibronectin since monoculture spheroids showed little expression in comparison to double and triple co-cultures. Additionally, visual changes in the fibronectin deposition from the double culture to the triple culture conditions were not observed.

Finally, all these results allowed a solid characterization of a triple co-culture MCTS model that better recapitulates avascular breast cancer. However, some aspects should be further addressed such as macrophage polarization into M1 or M2 macrophages, since CD68 identifies both phenotypes.

Co-culture spheroids comprising MCF-7 cells and fibroblasts [104], as well as MCF-7 cells and macrophages [117] have been previously established, enabling the study of the interaction between these different cell types. However, this model constitutes an improvement in comparison to the formers as it additionally enables the study of the crosstalk between fibroblasts and immune cells and the impact that these heterotypic interactions have on breast cancer progression. For instance, CAFs play a role in monocyte recruitment and differentiation into macrophages, by secreting CCL12, while immune cells secrete TGF-β that promotes fibroblast migration, proliferation and transdifferentiation into myofibroblasts [58, 104].

4.4 Nanoparticles production and characterization

Once the characterization of the triple culture MCTS was completed, the feasibility of the model developed as a platform for drug screening was tested. Firstly, a previously optimized nanoformulation was prepared by nanoprecipitation [96] and characterized by dynamic light scattering.

This nanosystem consisted in PLGA NPs loaded with GEF, a tyrosine kinase inhibitor of the intracellular domain of epidermal growth factor receptor (EGFR) [118]. Though only currently approved for the treatment of lung cancer by the FDA [119], several studies have been addressing the therapeutic impact of this drug in breast cancer, with some promising results obtained for luminal A breast cancer [4, 5]. Indeed, EGFR is expressed in several breast cancer subtypes and cell lines, including MCF-7 [120]. Moreover, PLGA is a polymer which has been approved by the FDA for the use in drug delivery applications because of its versatility, as well as biocompatibility and biodegradability properties [121].

Regarding their characterization, both bare and GEF-loaded NPs (NPs-GEF) were prepared and characterized regarding their Z-average size, polydispersity index (PdI) and surface charge (ζ-potential), as shown in Table 1. The results were, in general, consistent with the values formerly obtained, though a slight increase in the size and PdI of the NP samples was observed. Indeed, the most commonly accepted values, in terms of PdI, for polymeric nanoparticles are usually below 0.2 [48], which was not achieved in the case of GEF-encapsulated NPs. Regarding the ζ-potential, the values were similar to the ones priorly reported. Importantly, while the majority of the studies report a higher internalization efficiency of positively charged NPs by cells (mainly due to the electrostatic interactions established with the negatively charged cell membrane), other studies have reported an efficient cellular internalization of nanoparticles with a negative surface charge [122, 123]. Furthermore, the NPs produced with this protocol have previously shown high interaction with more than one cancer cell line [96].

Concerning the evaluation of other parameters, such as the association efficiency (AE) and the drug loading (DL) capacity, the values considered were the ones obtained in the former study, as these parameters were not assessed in this work. Hence, the values of AE and DL reported for NPs-GEF were 74 ± 5% and 4 ± 0%, respectively [96].

Table 3 Physicochemical properties of the empty and gefitinib-loaded NPs produced. Values are represented as: mean ± SD (n = 3).

	Z-average size (nm)	**PdI**	**ζ-potential (mV)**
Empty NPs	83 ± 2	0.191 ± 0.005	-12.0 ± 0.2
Gefitinib-loaded NPs	77 ± 2	0.233 ± 0.003	-10.8 ± 1.4

4.5 Evaluation of gefitinib nanoparticles therapeutic efficacy in established breast cancer 3D model

The NPs prepared were incubated with the 3D triple MCTS model formerly established for 24 h and 48 h, 7 days after spheroid assembly. Different therapeutic groups were tested in order to better understand the influence of each component in the nanosystem. Therefore, the MCTS were incubated with empty NPs, GEF-loaded NPs and free GEF. With the objective of performing a drug-response study, 3 different concentrations of GEF were tested for each condition: 2.2 μg/mL, 11.0 μg/mL and 22.0 μg/mL. The concentrations were chosen considering a previous study demonstrating the cytotoxic effect of GEF on MCF-7 cells [124]. Moreover, the concentration of PLGA NPs used was also taken into consideration, since previous studies from colleagues demonstrated cytotoxic effects starting at a concentration of 1000.0 μg/mL [96]. As a negative control, MCTS were incubated solely with complete culture media. Additionally, to comprehend how the 3D cellular organization, as well as the heterotypic interactions could potentially affect the response of the cells to the treatment, MCF-7 cells alone, cultured in a 2D system, were incubated in all the conditions described above.

At specific timepoints (24 h and 48 h after treatment initiation), the metabolic activity of the 2D and 3D cells was assessed through the resazurin assay. Moreover, 24 h after incubation, a live/dead assay was performed to evaluate cell viability upon treatment with different therapeutic approaches. For the 3D MCTS, an additional assay was carried out after 48 h of incubation, which consisted in indirectly evaluating cell viability by measuring the amount of ATP generated by the spheroids.

Starting with the results obtained for the 2D MCF-7 cell culture, after 24 h of treatment, empty NPs did not apparently impact the metabolic levels when compared to the untreated cells, suggesting that these concentrations are not cytotoxic throughout this time period (Figure 11A). At the second timepoint (48 h), however, bare NPs seem to decrease the metabolic activity of the cells at the higher concentrations (Figure 11B). Therefore, these results may suggest that NP concentrations above 500.0 μg/mL possibly display a cytotoxic effect in these cells. Regarding the free administration of GEF, this therapeutic approach was seemingly associated with the lowest metabolic activity of the cells, regardless of the concentration tested or the incubation time. In addition, the cells treated with GEF-loaded NPs apparently decreased their metabolic activity after 48 h of incubation. These results suggest that free GEF was, in general, the treatment that presented the highest cytotoxic effect on the cells. Even though the treatment with NPs-GEF also decreased the metabolic activity of the cells, especially after 48 h of incubation, this effect seems to be partially attributed to the cytotoxic effect observed for the bare NPs. It is important to note that, according to the International Organization for Standardization (ISO) guidelines for cytotoxicity in medical devices, a cytotoxic effect is only observed when there is a reduction of cell viability by more than 30% [125].

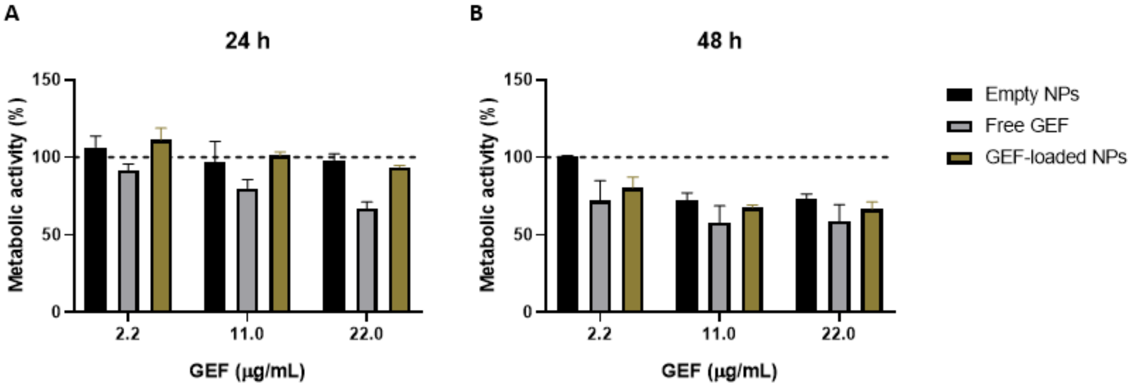

Figure 11 Evaluation of the relative metabolic activity of treated MCF-7 cells in relation to the non-treated cells (100% viability), culture in 2D, at **A)** 24 h and **B)** 48 h after treatment initiation with different therapeutic approaches. The concentrations of GEF correspond to 2.2 µg/mL, 11.0 µg/mL and 22.0 µg/mL. The concentrations of NPs correspond to 100.0 µg/mL, 500.0 µg/mL and 1000.0 µg/mL. Values represent mean ± SD (n =3 per condition, 1 independent experiment).

To complement the results of the resazurin assay, a live/dead cell staining was performed after 24 h of treatment. The results showed that non-treated cells and cells treated with the lowest concentration of bare NPs were the only conditions in which dead cells were not visible. In opposite to what was observed in the resazurin assay at 24 h, NPs-GEF apparently induced a cytotoxic effect on the cells after 24 h. Moreover, the number of dead cells was higher upon treatment with NPs-GEF than with free GEF, especially when comparing the two highest concentrations, which also contrasts with what was observed in the resazurin assay. In fact, in those two conditions (NPs-GEF 11.0 µg/mL and NPs-GEF 22.0 µg/mL), cells showed a less confluent stage, suggesting that NPs-GEF could affect the proliferation rate of the cells. These results were not expected since NPs-GEF enable a more controlled release of the drug [96]. While this could be explained by a synergistic effect caused by GEF and bare NPs cytotoxicity, these results should have translated into those of the metabolic levels assessed through the resazurin assay. However, that was not observed, so the experiments should be repeated to validate the results.

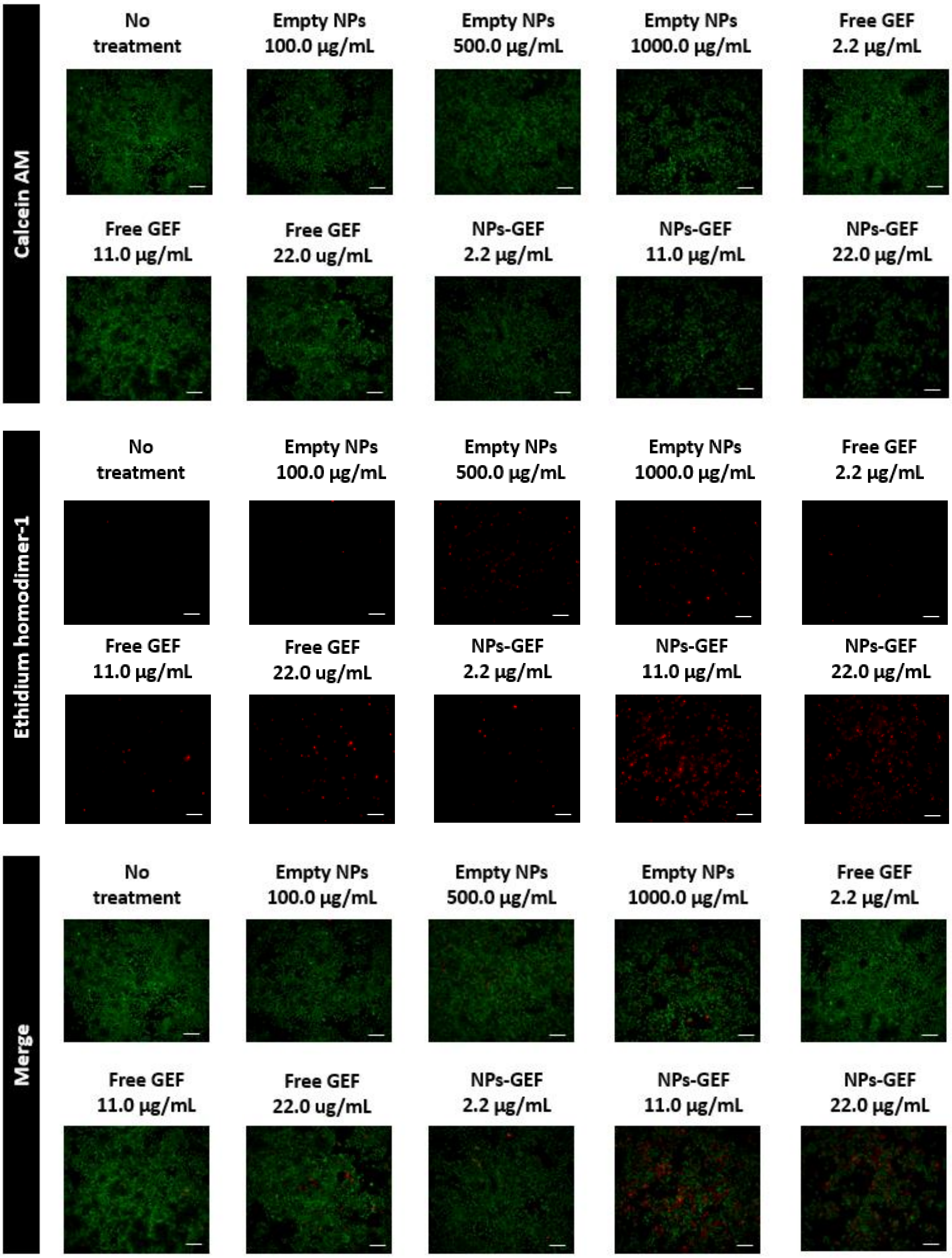
Calcein AM
No treatment
Empty NPs 100.0 µg/mL
Empty NPs 500.0 µg/mL
Empty NPs 1000.0 µg/mL
Free GEF 2.2 µg/mL
Free GEF 11.0 µg/mL
Free GEF 22.0 ug/mL
NPs-GEF 2.2 µg/mL
NPs-GEF 11.0 µg/mL
NPs-GEF 22.0 µg/mL
Ethidium homodimer-1
No treatment
Empty NPs 100.0 µg/mL
Empty NPs 500.0 µg/mL
Empty NPs 1000.0 µg/mL
Free GEF 2.2 µg/mL
Free GEF 11.0 µg/mL
Free GEF 22.0 ug/mL
NPs-GEF 2.2 µg/mL
NPs-GEF 11.0 µg/mL
NPs-GEF 22.0 µg/mL
Merge
No treatment
Empty NPs 100.0 µg/mL
Empty NPs 500.0 µg/mL
Empty NPs 1000.0 µg/mL
Free GEF 2.2 µg/mL
Free GEF 11.0 µg/mL
Free GEF 22.0 ug/mL
NPs-GEF 2.2 µg/mL
NPs-GEF 11.0 µg/mL
NPs-GEF 22.0 µg/mL

Figure 12 Cell viability assessment of the 2D MCF-7 cell culture through a live/dead assay using calcein AM and EthD-1 to stain live and dead cells, respectively. The assay was performed 24 h after treatment initiation. The concentrations of GEF correspond to 2.2 µg/mL, 11.0 µg/mL and 22.0 µg/mL. The concentrations of NPs correspond to 100.0 µg/mL, 500.0 µg/mL and 1000.0 µg/mL. Green channel: calcein AM; red channel: EthD-1. Scale bars represent 50 µm.

Regarding the metabolic activity analysis of the 3D triple culture MCTS (Figure 13), results seem to indicate that empty NPs do not impact the metabolic activity of these structures regardless of the concentration, unlike what was observed for the 2D cell culture. This is consistent with previous studies that reported that the 3D conformation of the MCTS can hamper NPs penetration into the tissue [126]. In agreement with the 2D cell culture results, free administration of GEF was the therapeutic approach associated with the lowest metabolic activity, in a dose-dependent manner, after 24 h and 48 h of treatment. In turn, spheroids incubated with the highest concentration of NPs-GEF also seemingly presented a decrease in the metabolic activity after 24 h of incubation, but not after 48 h of treatment. This was not expected, as the metabolic levels should have at least been maintained, if not further reduced.

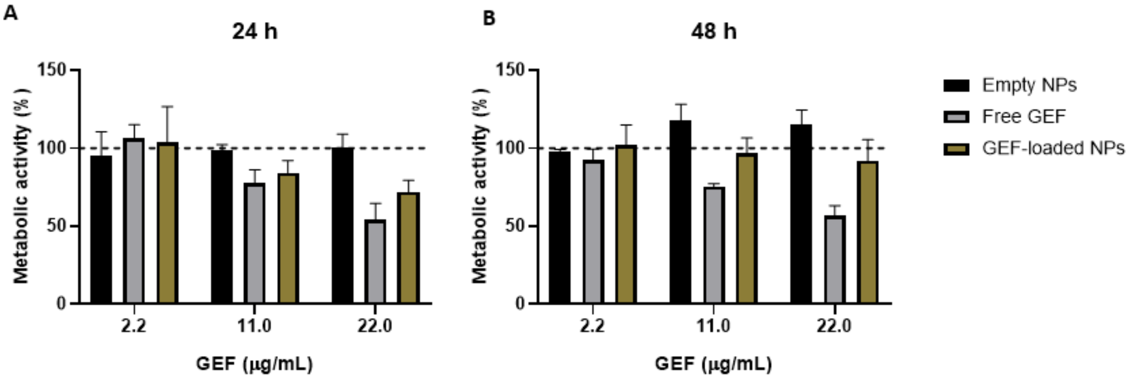

Figure 13 Evaluation of the relative metabolic activity of treated 3D triple culture MCTS in relation to the non-treated spheroids (100% viability) at **A)** 24 h and **B)** 48 h after treatment initiation with different therapeutic approaches. The concentrations of GEF correspond to 2.2 µg/mL, 11.0 µg/mL and 22.0 µg/mL. The concentrations of NPs correspond to 100.0 µg/mL, 500.0 µg/mL and 1000.0 µg/mL. Values represent mean ± SD (n=3 spheroids per condition, 2 independent experiments).

Additionally, to complement this analysis, another cell viability assay was performed for the evaluation of cell toxicity using 3D CellTiter-Glo® reagent, which enables the quantification of the ATP levels generated by the MCTS. This is an indirect method to assess cell viability, as the measurement of ATP levels is proportional to the number of viable cells. The present assay was performed 48 h after incubation. A first look at the results suggests that NPs-GEF impacted cell viability in a similar way to free GEF administration, unlike to what was observed in the resazurin assay. This assay seems to be a more sensitive method to evaluate cell viability than the previous one, as the percentage of cell viability reduction was more pronounced. Indeed, this reagent is specific for the use in 3D models, unlike resazurin which is more used in 2D cell cultures.

Moreover, unlike what was observed in the 2D culture, this assay apparently suggests that NPs-GEF contributed to a higher impact on cell viability than free GEF at lower concentrations. While this could be unexpected, since NPs penetration is usually hampered in 3D structures, the crosstalk between the different cells that constitute the MCTS may contribute to a higher cytotoxic effect at lower concentrations. For instance, the phagocytic nature of macrophages could contribute to a higher uptake of the NPs, therefore justifying these results [127]. As such, it would be important to additionally perform these assays in treated 2D-cultured macrophages and fibroblasts, in order to have a better perspective of the interaction of each of these cell types with the NPs, including their role in NP uptake.

Additionally, studies from colleagues that assessed the therapeutic efficacy of Nutlin-3a-loaded spermine-modified acetalated dextran (Sp-AcDEX) NPs in a triple co-culture MCTS comprising the HCT116 human colorectal cancer cell line also reported a more prominent effect of the NPs used in the 3D MCTS model than in the 2D monolayers [95].

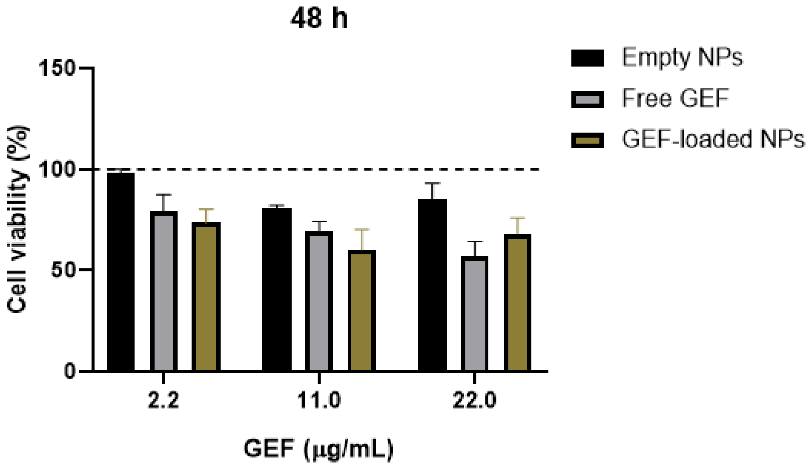

Figure 14 Evaluation of the relative 3D triple culture MCTS cell activity in relation to the non-treated spheroids (100% viability) at 48 h after treatment initiation with different therapeutic approaches. The concentrations of GEF correspond to 2.2 μg/mL, 11.0 μg/mL and 22.0 μg/mL. The concentrations of NPs correspond to 100.0 μg/mL, 500.0 μg/mL and 1000.0 μg/mL. Values represent mean ± SD (n =3 spheroids per condition, 2 independent experiments).

In contrast, cell viability assessment in the MCTS, through live/dead assay (Figure 15), suggested that NPs-GEF do not cause a prominent cytotoxic effect, as cell death is not observed at 24 h of treatment. Additionally, treatment with free GEF also did not cause considerable cell death, except for the 11.0 μg/mL concentration. Considering the fact that free GEF has been reported to display a cytotoxic effect on MCF-7 cells [124] – and since that effect was also observed in the 2D cell culture –, these results may indicate that this assay needs to be further optimized as the dyes may not be able to infiltrate the MCTS during the incubation time considered for this assay.

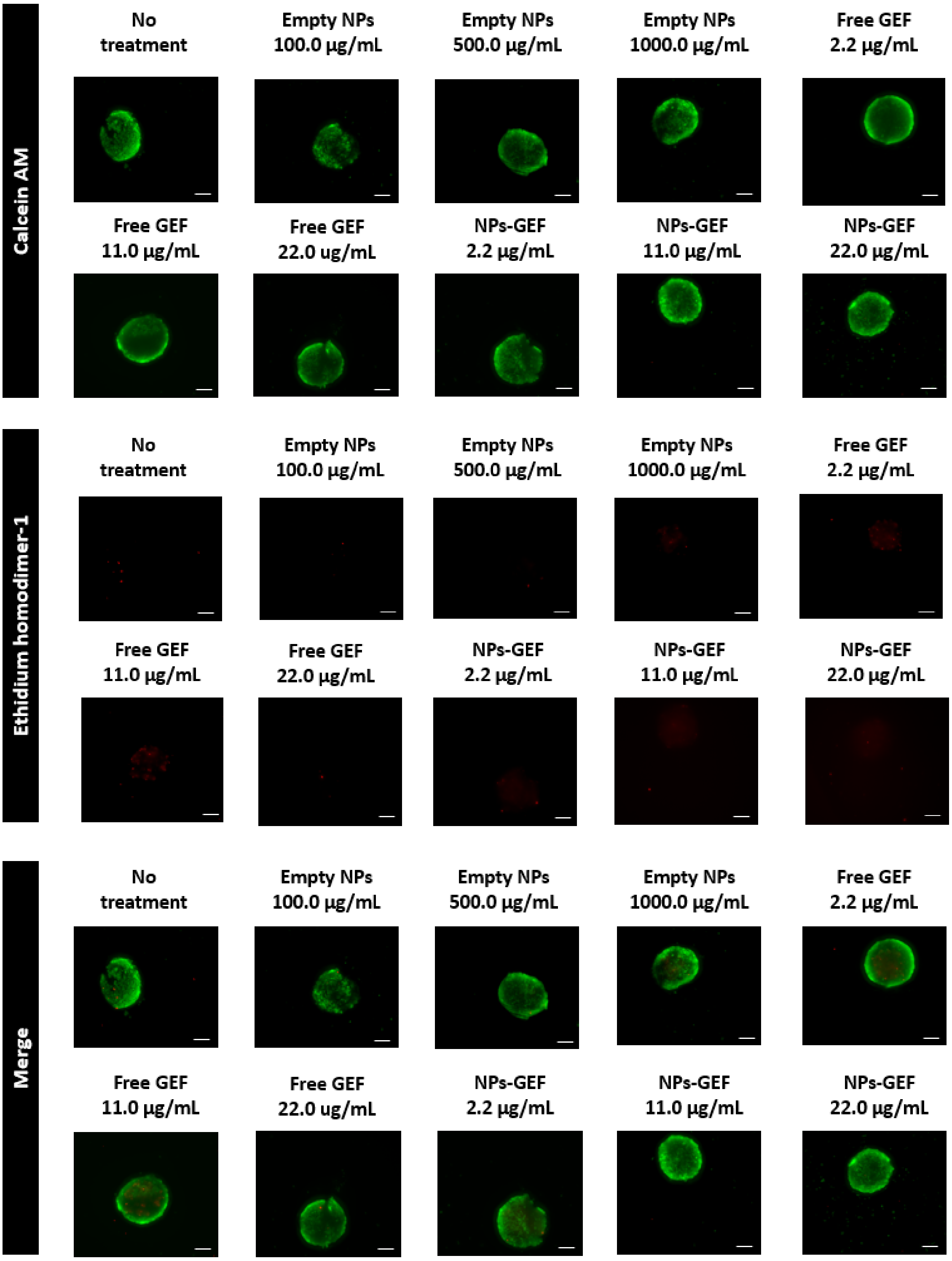
Calcein AM
No treatment
Empty NPs 100.0 µg/mL
Empty NPs 500.0 µg/mL
Empty NPs 1000.0 µg/mL
Free GEF 2.2 µg/mL
Free GEF 11.0 µg/mL
Free GEF 22.0 ug/mL
NPs-GEF 2.2 µg/mL
NPs-GEF 11.0 µg/mL
NPs-GEF 22.0 µg/mL
Ethidium homodimer-1
No treatment
Empty NPs 100.0 µg/mL
Empty NPs 500.0 µg/mL
Empty NPs 1000.0 µg/mL
Free GEF 2.2 µg/mL
Free GEF 11.0 µg/mL
Free GEF 22.0 µg/mL
NPs-GEF 2.2 µg/mL
NPs-GEF 11.0 µg/mL
NPs-GEF 22.0 µg/mL
Merge
No treatment
Empty NPs 100.0 µg/mL
Empty NPs 500.0 µg/mL
Empty NPs 1000.0 µg/mL
Free GEF 2.2 µg/mL
Free GEF 11.0 µg/mL
Free GEF 22.0 ug/mL
NPs-GEF 2.2 µg/mL
NPs-GEF 11.0 µg/mL
NPs-GEF 22.0 µg/mL

Figure 15 Cell viability assessment of the 3D MCTS through a live/dead assay using calcein AM and EthD-1 to stain live and dead cells, respectively. The assay was performed 24 h after treatment initiation. The concentrations of GEF correspond to 2.2 µg/mL, 11.0 µg/mL and 22.0 µg/mL. The concentrations of NPs correspond to 100.0 µg/mL, 500.0 µg/mL and 1000.0 µg/mL. Green channel: calcein AM; red channel: EthD-1. Scale bar represents 50 µm.

Considering all the results obtained, a few conclusions can be drawn. Firstly, while in the 2D culture the empty NPs seemed to display a cytotoxic effect on the cells (especially at higher concentrations and after 48 h of incubation), 3D MCTS cell viability is apparently not affected by this interaction. As formerly mentioned, this is likely explained by the reduced capacity of the

NPs to penetrate 3D structures. Additionally, the tumor ECM present in these structures (as previously seen by immunohistochemistry staining) may contribute to the limited NP infiltration, since it has been reported that tumor ECM constitutes a physical barrier for the drug, as it is much denser and less organized than normal ECM [86]. Therefore, the cytotoxic effect displayed by NPs-GEF in 2D cells may be partially attributed to the NPs, whereas, in the MCTS, the cytotoxic effect of this treatment is most likely due to the drug that is being released overtime.

Secondly, while it would be expected that the free GEF would display a higher impact on cell viability than NPs-GEF, as the latter displays a more controlled release of the drug, in the 3D MCTS, these therapies had similar impacts on cell viability, according to the CellTiter Glo® reagent assay, which seems to display the most feasible results out of the methods performed. This indicates that GEF is indeed being released by the NPs.

Finally, the heterotypic interactions between the cells incorporated in the MCTS most likely affect the NP uptake, as well its therapeutic effect. For instance, macrophages may promote the NP uptake. However, cells present in the TME, including TAMs and CAFs have also been reported to promote drug resistance in tumor cells [128]. Therefore, these results further support the need to recapitulate the hallmarks of TME in the pre-clinical models used for drug screening studies, so as to achieve more feasible outcomes.

Nevertheless, to further validate these results, a higher number of patients should be used in order to obtain more robust outcomes. Moreover, it could be important to study the effect of these treatments in fibroblasts and monocytes cultured in 2D, in order to further understand their impact in the therapeutic efficacy of this treatment. Additionally, NPs could be labelled with a fluorescent dye in order to further understand their interaction with the cells.

Chapter 5

Conclusion

5.1 Concluding remarks

Breast cancer is one of most predominant and lethal cancers worldwide, which explains the constant search for more efficient therapies that effectively treat this disease. However, the majority of the *in vitro* models used in the process of drug discovery poorly recapitulates crucial features of the breast TME, such as the spatial architecture, along with cell-cell and cell-matrix interactions. Moreover, although *in vivo* animal models are extremely important in this process, they significantly increase its cost and length [3]. All things considered, 3D models represent a valuable tool to simultaneously minimize the costs associated with the use of animals and better reproduce, *in vitro*, the essential characteristics of breast tumors.

Therefore, the main goal of this dissertation was the establishment and characterization of a triple co-culture 3D breast cancer spheroid model that not only reproduces the tumor spatial cell organization but also incorporates key cellular components of the breast TME (such mammary fibroblasts and macrophages) that play important roles in cancer progression, as well as in the tumor's response to treatment. Overall, this objective was successfully achieved. Nevertheless, other studies could be performed in order to further characterize this model, for instance in regards to macrophage polarization. Moreover, it would be important to repeat some of the experiments performed, with more human blood donors, in order to improve the robustness of the results.

Additionally, the implementation of this model as a platform for drug screening constituted another important goal of this dissertation. As such, the validation of the triple co-culture MCTS was achieved by treatment with GEF, a drug that has previously shown a cytotoxic effect in the MCF-7 breast cancer cell line [5, 124]. Further, the MCTS were treated with a nano-based drug system, previously optimized by colleagues, comprising NPs loaded with GEF, in order to evaluate the efficacy of this therapeutic approach in the model developed. Overall, these results indicate that NPs-GEF may display, to some extent, a cytotoxic effect in the MCTS.

In conclusion, the work developed throughout this dissertation constitutes an important advance in the development of more complex models that mimic breast cancer. Moreover, it opens the possibility to use this model as a validation tool regarding the therapeutic efficacy of different nanotherapies against breast cancer, including the NPs-GEF treatment tested in this work.

5.2 Future perspectives

One of the main limitations of this model is the fact that it is an avascular structure, and therefore does not take into consideration a very important aspect that contributes to tumor growth: angiogenesis. Hence, following the complete characterization of this model, the MCTS could be further incorporated into more complex structures, such as tumor-on-chips, to better recapitulate this important hallmark in cancer progression. Another possibility could be to add endothelial cells to the model. Moreover, other immune cell types could be added in order to test the efficacy of combined chemoimmunotherapy in the model developed.

As previously discussed, the localization of the fibroblasts in this model was not very representative of the clinical situation. Therefore, the MCTS could be further optimized by testing other cell seeding approaches that contribute to a more clinically relevant model.

Furthermore, considering the high heterogeneity of breast cancer, it would be important to optimize this model for different breast cancer cell lines, in order to obtain a wider representation of the remaining subtypes. Additionally, as different breast cancer subtypes express different levels of EGFR, it would be interesting to test the treatment with GEF-loaded NPs in other subtypes, especially in triple negative breast cancers, which are usually characterized by high EGFR expression levels [129].

Appendix A

Characterization of double co-culture MCF-7:hMF MCTS (2,500 cells/spheroid)

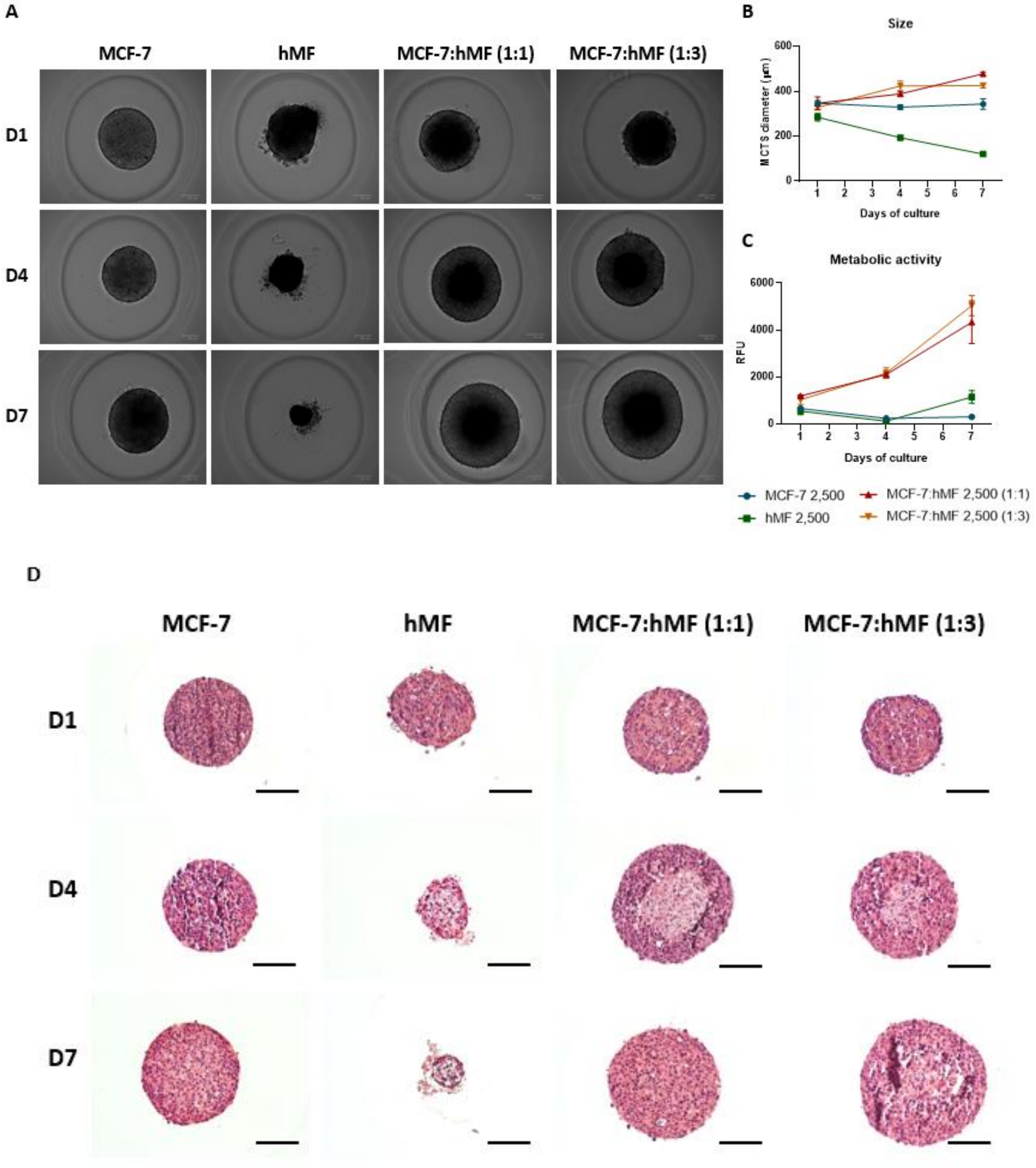
A
MCF-7
hMF
MCF-7:hMF (1:1)
MCF-7:hMF (1:3)
D1
D4
D7
B
Size
MCTS diameter (µm)
600
400
200
0
1 2 3 4 5 6 7
Days of culture
C
Metabolic activity
RFU
6000
4000
2000
0
1 2 3 4 5 6 7
Days of culture
MCF-7 2,500
hMF 2,500
MCF-7:hMF 2,500 (1:1)
MCF-7:hMF 2,500 (1:3)
D
MCF-7
hMF
MCF-7:hMF (1:1)
MCF-7:hMF (1:3)
D1
D4
D7

Figure 16 Characterization of MCF-7:hMF double co-culture MCTS, assembled at the initial cell density of 2,500 cells/spheroid, over seven days of culture. Two cellular ratios of MCF-7 cells to hMFs were tested – 1:1 and 1:3. MCF-7 and hMF monoculture MCTS were cultured as control spheroids. **A)** Brightfield microscopy images of the MCTS morphology, taken at days 1, 4 and 7 after cell seeding. Scale bar represents 100 µm. **B)** Measurement of the MCTS diameter from the brightfield images taken. Values represent mean ± SD (n = 5 spheroids per condition, 1 independent experiment). **C)** Evaluation of the MCTS metabolic activity at the formerly mentioned timepoints, according to the initial cell density. Values represent mean ± SD (n=81 spheroids per condition, 1 independent experiment). RFU: relative fluoresce units. **D)** Histological analysis by H&E staining of the MCTS overtime. Scale bar represents 100 µm.

Appendix B

Detailed immunostaining analysis of monoculture, double culture and triple culture MCTS

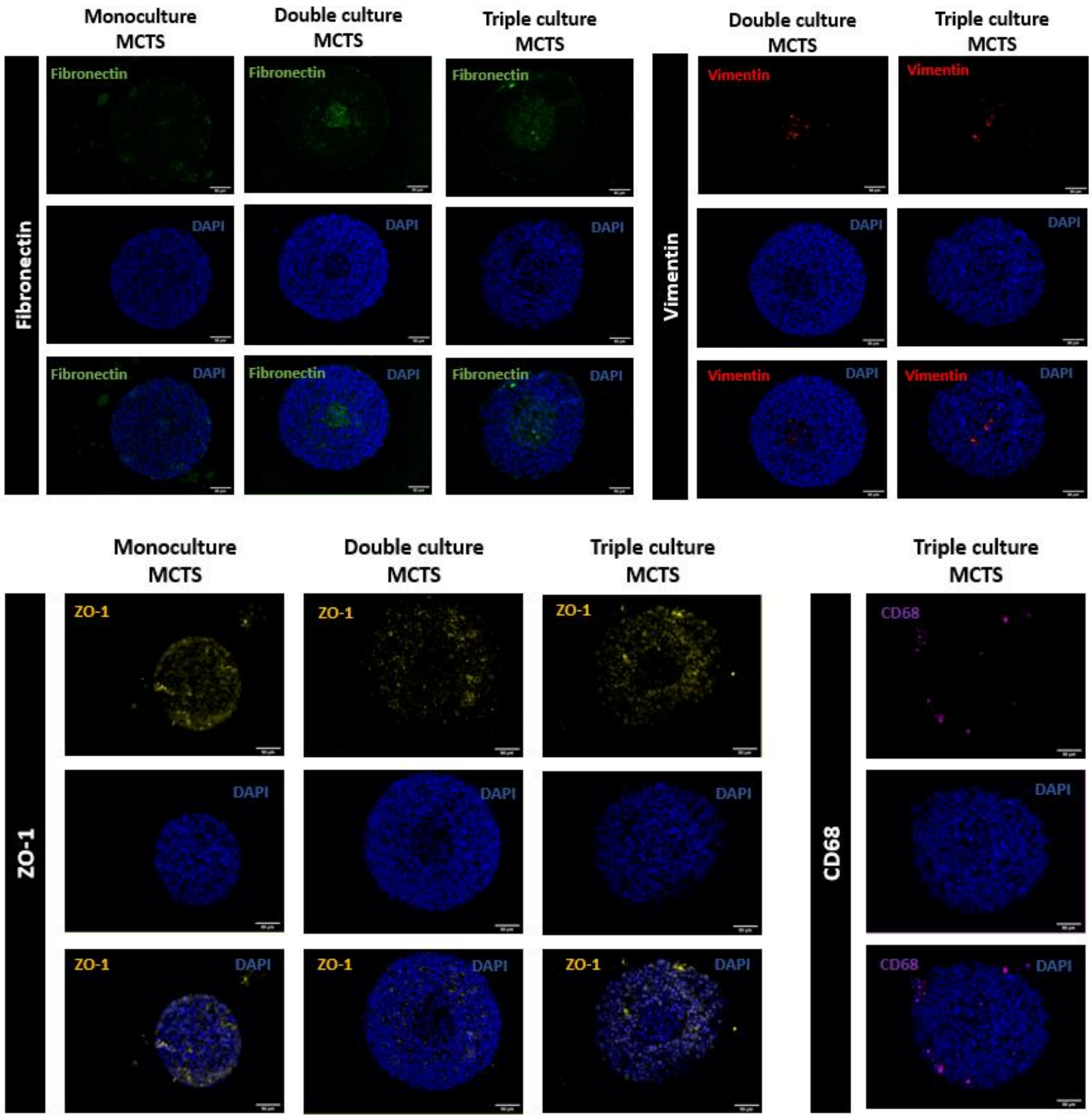
Monoculture MCTS
Double culture MCTS
Triple culture MCTS
Double culture MCTS
Triple culture MCTS
Fibronectin
Fibronectin
DAPI
Fibronectin
DAPI
Vimentin
Vimentin
DAPI
Vimentin
DAPI
Monoculture MCTS
Double culture MCTS
Triple culture MCTS
Triple culture MCTS
ZO-1
ZO-1
DAPI
ZO-1
DAPI
CD68
CD68
DAPI
CD68
DAPI

Figure 17 Detailed immunofluorescence microscopy images of mono-, double and triple culture MCTS at day 7 after cell seeding. Fibronectin (green); ZO-1 (yellow); Vimentin (red); CD68 (violet). All samples are counterstained with DAPI (blue channel). Scale bar represents 50 µm.

Appendix C

Effect of different culture media in the metabolic activity and size of 3D MCF-7 MCTS

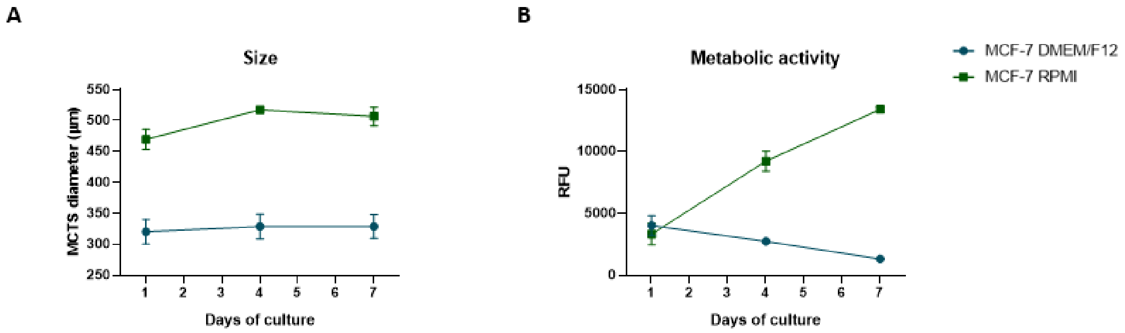

Figure 18 Comparison study between MCF-7 monoculture MCTS seeded in different culture media at the cellular concentration of 5,000 cells/ spheroid, regarding their **A)** metabolic activity and **B)** size. RFU: relative fluorescence units.

Appendix D

E-cadherin staining of triple co-culture MCTS by flow cytometry

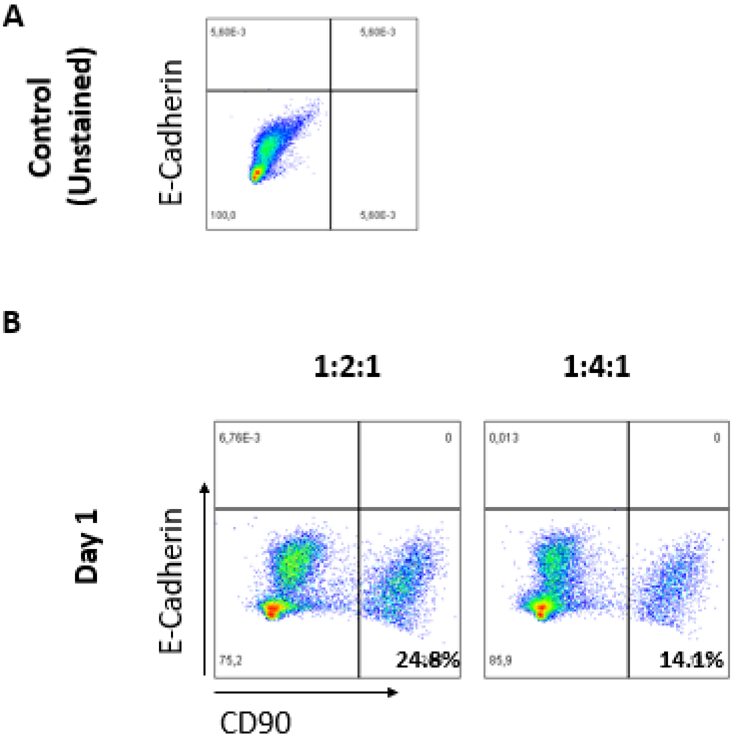

Figure 19 MCF-7 characterization of MCF-7:monocytes:hMF triple co-culture MCTS, assembled at the initial cell density of 5,000 cells/spheroid, by flow cytometry. **A)** E-cadherin$^+$ cells were gated on live dead negative cells. **B)** Two cellular ratios of MCF-7 cells to monocytes to hMFs were tested – 1:2:1 and 1:4:1, at day 1 and day 7 of culture. Numbers indicate the percentage of the previously cited populations

Appendix E

Quantitative results on the live/dead assay performed to characterize the triple co-culture MCTS

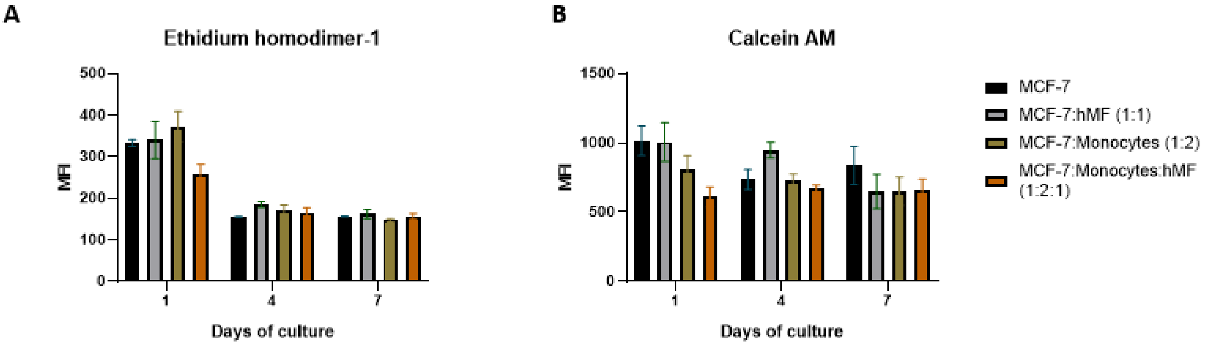

Figure 20 Quantitative results of the calcein AM and EthD-1 fluorescence intensities regarding different spheroid conditions measured at days 1, 4 and 7 after cell seeding. MFI: Mean fluorescence intensity.

References

1. Sung, H., et al., *Global Cancer Statistics 2020: GLOBOCAN Estimates of Incidence and Mortality Worldwide for 36 Cancers in 185 Countries.* CA Cancer J Clin, 2021. **71**(3): p. 209-249 DOI: 10.3322/caac.21660.
2. Luque-Bolivar, A., et al., *Resistance and Overcoming Resistance in Breast Cancer.* Breast Cancer (Dove Med Press), 2020. **12**: p. 211-229 DOI: 10.2147/bctt.S270799.
3. Zanoni, M., et al., *Modeling neoplastic disease with spheroids and organoids.* J Hematol Oncol, 2020. **13**(1): p. 97 DOI: 10.1186/s13045-020-00931-0.
4. Gee, J.M., et al., *The antiepidermal growth factor receptor agent gefitinib (ZD1839/Iressa) improves antihormone response and prevents development of resistance in breast cancer in vitro.* Endocrinology, 2003. **144**(11): p. 5105-17 DOI: 10.1210/en.2003-0705.
5. Jeong, Y., et al., *EGFR is a Therapeutic Target in Hormone Receptor-Positive Breast Cancer.* Cell Physiol Biochem, 2019. **53**(5): p. 805-819 DOI: 10.33594/000000174.
6. Siegel, R.L., et al., *Cancer Statistics, 2021.* CA Cancer J Clin, 2021. **71**(1): p. 7-33 DOI: 10.3322/caac.21654.
7. Organization, W.H. *Breast Cancer*. 2021 22/05/2021]; Available from: https://www.who.int/news-room/fact-sheets/detail/breast-cancer.
8. Lawrence, R.A. and R.M. Lawrence, *Chapter 2 - Anatomy of the human breast*, in *Breastfeeding (Sixth Edition)*, R.A. Lawrence and R.M. Lawrence, Editors. 2005, Mosby: Philadelphia. p. 39-63.
9. National Breast Cancer Foundation, I. *Breast Anatomy*. 2021 29/05/2021]; Available from: https://www.nationalbreastcancer.org/breast-anatomy.
10. Center, M.S.K.C. *Anatomy of the Breast* 2021 20/05/2021]; Available from: https://www.mskcc.org/cancer-care/types/breast/anatomy-breast.
11. Khan, Y.S. and H. Sajjad, *Anatomy, Thorax, Mammary Gland*, in *StatPearls*. 2021, StatPearls Publishing Copyright © 2021, StatPearls Publishing LLC.: Treasure Island (FL).
12. UK, C.R. *Breast Cancer Symptons*. 2020 27/05/2021]; Available from: https://www.cancerresearchuk.org/about-cancer/breast-cancer/symptoms.
13. Coughlin, S.S., *Epidemiology of Breast Cancer in Women*, in *Breast Cancer Metastasis and Drug Resistance: Challenges and Progress*, A. Ahmad, Editor. 2019, Springer International Publishing: Cham. p. 9-29.
14. Momenimovahed, Z. and H. Salehiniya, *Epidemiological characteristics of and risk factors for breast cancer in the world.* Breast Cancer (Dove Med Press), 2019. **11**: p. 151-164 DOI: 10.2147/bctt.S176070.
15. Shah, R., K. Rosso, and S.D. Nathanson, *Pathogenesis, prevention, diagnosis and treatment of breast cancer.* World J Clin Oncol, 2014. **5**(3): p. 283-98 DOI: 10.5306/wjco.v5.i3.283.
16. Martin, A.M. and B.L. Weber, *Genetic and hormonal risk factors in breast cancer.* J Natl Cancer Inst, 2000. **92**(14): p. 1126-35 DOI: 10.1093/jnci/92.14.1126.
17. Institute, N.C. *Breast Cancer Screening (PDQ®)–Patient Version*. 2021 30/05/2021]; Available from: https://www.cancer.gov/types/breast/patient/breast-screening-pdq.
18. Society, A.C. *American Cancer Society Recommendations for the Early Detection of Breast Cancer*. 2021 02/06/2021]; Available from: https://www.cancer.org/cancer/breast-cancer/screening-tests-and-early-detection/american-cancer-society-recommendations-for-the-early-detection-of-breast-cancer.html.

19. Vahabi, M., *Breast cancer screening methods: a review of the evidence.* Health Care Women Int, 2003. **24**(9): p. 773-93 DOI: 10.1080/07399330390229957.
20. Vuong, D., et al., *Molecular classification of breast cancer.* Virchows Arch, 2014. **465**(1): p. 1-14 DOI: 10.1007/s00428-014-1593-7.
21. Malhotra, G.K., et al., *Histological, molecular and functional subtypes of breast cancers.* Cancer Biol Ther, 2010. **10**(10): p. 955-60 DOI: 10.4161/cbt.10.10.13879.
22. Fahad Ullah, M., *Breast Cancer: Current Perspectives on the Disease Status*, in *Breast Cancer Metastasis and Drug Resistance: Challenges and Progress*, A. Ahmad, Editor. 2019, Springer International Publishing: Cham. p. 51-64.
23. Akram, M., et al., *Awareness and current knowledge of breast cancer.* Biol Res, 2017. **50**(1): p. 33 DOI: 10.1186/s40659-017-0140-9.
24. Sinn, H.-P. and H. Kreipe, *A Brief Overview of the WHO Classification of Breast Tumors, 4th Edition, Focusing on Issues and Updates from the 3rd Edition.* Breast care (Basel, Switzerland), 2013. **8**(2): p. 149-154 DOI: 10.1159/000350774.
25. Nascimento, R. and K. Otoni, *Histological and molecular classification of breast cancer: what do we know?* Mastology, 2020. **30** DOI: 10.29289/25945394202020200024.
26. Santen, R., L. Duska, and S. Culp. *Chapter 29@ Hormone Responsive Cancers*. 2014.
27. Gutierrez, C. and R. Schiff, *HER2: biology, detection, and clinical implications.* Arch Pathol Lab Med, 2011. **135**(1): p. 55-62 DOI: 10.5858/2010-0454-rar.1.
28. Untch, M., et al., *13th st. Gallen international breast cancer conference 2013: primary therapy of early breast cancer evidence, controversies, consensus - opinion of a german team of experts (zurich 2013).* Breast Care (Basel), 2013. **8**(3): p. 221-9 DOI: 10.1159/000351692.
29. Boix-Montesinos, P., et al., *The past, present, and future of breast cancer models for nanomedicine development.* Adv Drug Deliv Rev, 2021. **173**: p. 306-330 DOI: 10.1016/j.addr.2021.03.018.
30. Breatcancer.org. *Molecular Subtypes of Breast Cancer*. 2021 08/06/2021]; Available from: https://www.breastcancer.org/symptoms/types/molecular-subtypes.
31. Anders, C.K. and L.A. Carey, *Biology, metastatic patterns, and treatment of patients with triple-negative breast cancer.* Clin Breast Cancer, 2009. **9 Suppl 2**(Suppl 2): p. S73-81 DOI: 10.3816/CBC.2009.s.008.
32. Dai, X., et al., *Breast cancer intrinsic subtype classification, clinical use and future trends.* American journal of cancer research, 2015. **5**(10): p. 2929-2943.
33. Waks, A.G. and E.P. Winer, *Breast Cancer Treatment: A Review.* JAMA, 2019. **321**(3): p. 288-300 DOI: 10.1001/jama.2018.19323.
34. Maughan, K.L., M.A. Lutterbie, and P.S. Ham, *Treatment of breast cancer.* Am Fam Physician, 2010. **81**(11): p. 1339-46.
35. *Mastectomy or lumpectomy? The choice of operation for clinical stages I and II breast cancer. The Steering Committee on Clinical Practice Guidelines for the Care and Treatment of Breast Cancer. Canadian Association of Radiation Oncologists.* Cmaj, 1998. **158 Suppl 3**: p. S15-21.
36. Alkabban, F.M. and T. Ferguson, *Breast Cancer*, in *StatPearls*. 2021, StatPearls Publishing Copyright © 2021, StatPearls Publishing LLC.: Treasure Island (FL).
37. Valachis, A., et al., *Partial breast irradiation or whole breast radiotherapy for early breast cancer: a meta-analysis of randomized controlled trials.* Breast J, 2010. **16**(3): p. 245-51 DOI: 10.1111/j.1524-4741.2010.00905.x.
38. Oncology, A.S.o.C. *Breast Cancer: Types of Treatment*. 2020 14/06/2021]; Available from: https://www.cancer.net/cancer-types/breast-cancer/types-treatment.
39. Yager, J.D. and N.E. Davidson, *Estrogen carcinogenesis in breast cancer.* N Engl J Med, 2006. **354**(3): p. 270-82 DOI: 10.1056/NEJMra050776.

40. Miller, W.R., *Biological rationale for endocrine therapy in breast cancer.* Best Pract Res Clin Endocrinol Metab, 2004. **18**(1): p. 1-32 DOI: 10.1016/s1521-690x(03)00044-7.
41. Farhan, M., et al., *Non-coding RNAs as Mediators of Tamoxifen Resistance in Breast Cancers*, in *Breast Cancer Metastasis and Drug Resistance: Challenges and Progress*, A. Ahmad, Editor. 2019, Springer International Publishing: Cham. p. 229-241.
42. FDA. *FDA approves neratinib for metastatic HER2-positive breast cancer*. 2020 23/06/2021]; Available from: https://www.fda.gov/drugs/resources-information-approved-drugs/fda-approves-neratinib-metastatic-her2-positive-breast-cancer.
43. Breastcancer.org. *Chemotherapy*. 2019 24/06/2021]; Available from: https://www.breastcancer.org/treatment/chemotherapy.
44. Wahba, H.A. and H.A. El-Hadaad, *Current approaches in treatment of triple-negative breast cancer.* Cancer Biol Med, 2015. **12**(2): p. 106-16 DOI: 10.7497/j.issn.2095-3941.2015.0030.
45. Society, A.C. *Chemotherapy for Breast Cancer*. 2019 26/06/2021]; Available from: https://www.cancer.org/cancer/breast-cancer/treatment/chemotherapy-for-breast-cancer.html.
46. Iyer, A.K., et al., *Role of integrated cancer nanomedicine in overcoming drug resistance.* Adv Drug Deliv Rev, 2013. **65**(13-14): p. 1784-802 DOI: 10.1016/j.addr.2013.07.012.
47. Ortíz, R., et al., *Nanomedicine to Overcome Multidrug Resistance Mechanisms in Colon and Pancreatic Cancer: Recent Progress.* Cancers, 2021. **13**(9) DOI: 10.3390/cancers13092058.
48. Danaei, M., et al., *Impact of Particle Size and Polydispersity Index on the Clinical Applications of Lipidic Nanocarrier Systems.* Pharmaceutics, 2018. **10**(2) DOI: 10.3390/pharmaceutics10020057.
49. Hami, Z., *A Brief Review on Advantages of Nano-based Drug Delivery Systems.* Annals of Military and Health Sciences Research, 2021. **In Press** DOI: 10.5812/amh.112274.
50. Society, A.C. *Immunotherapy for Breast Cancer*. 2021 01/07/2021]; Available from: https://www.cancer.org/cancer/breast-cancer/treatment/immunotherapy.html.
51. Pardoll, D.M., *The blockade of immune checkpoints in cancer immunotherapy.* Nat Rev Cancer, 2012. **12**(4): p. 252-64 DOI: 10.1038/nrc3239.
52. Riella, L.V., et al., *Role of the PD-1 pathway in the immune response.* Am J Transplant, 2012. **12**(10): p. 2575-87 DOI: 10.1111/j.1600-6143.2012.04224.x.
53. Akinleye, A. and Z. Rasool, *Immune checkpoint inhibitors of PD-L1 as cancer therapeutics.* Journal of Hematology & Oncology, 2019. **12**(1): p. 92 DOI: 10.1186/s13045-019-0779-5.
54. Breastcancer.org. *Immunotherapy*. 2021 03/07/2021]; Available from: https://www.breastcancer.org/treatment/immunotherapy.
55. Tchou, J. and J. Conejo-Garcia, *Chapter Three - Targeting the Tumor Stroma as a Novel Treatment Strategy for Breast Cancer: Shifting from the Neoplastic Cell-Centric to a Stroma-Centric Paradigm*, in *Advances in Pharmacology*, K.S.M. Smalley, Editor. 2012, Academic Press. p. 45-61.
56. Soysal, S.D., A. Tzankov, and S.E. Muenst, *Role of the Tumor Microenvironment in Breast Cancer.* Pathobiology, 2015. **82**(3-4): p. 142-52 DOI: 10.1159/000430499.
57. Mendoza-Almanza, G., et al., *Role of platelets and breast cancer stem cells in metastasis.* World J Stem Cells, 2020. **12**(11): p. 1237-1254 DOI: 10.4252/wjsc.v12.i11.1237.
58. Houthuijzen, J.M. and J. Jonkers, *Cancer-associated fibroblasts as key regulators of the breast cancer tumor microenvironment.* Cancer Metastasis Rev, 2018. **37**(4): p. 577-597 DOI: 10.1007/s10555-018-9768-3.
59. Aboussekhra, A., *Role of cancer-associated fibroblasts in breast cancer development and prognosis.* Int J Dev Biol, 2011. **55**(7-9): p. 841-9 DOI: 10.1387/ijdb.113362aa.
60. Luo, H., et al., *Cancer-associated fibroblasts: a multifaceted driver of breast cancer progression.* Cancer Lett, 2015. **361**(2): p. 155-63 DOI: 10.1016/j.canlet.2015.02.018.

61. Orimo, A., et al., *Stromal fibroblasts present in invasive human breast carcinomas promote tumor growth and angiogenesis through elevated SDF-1/CXCL12 secretion.* Cell, 2005. **121**(3): p. 335-48 DOI: 10.1016/j.cell.2005.02.034.
62. Batlle, E. and J. Massagué, *Transforming Growth Factor-β Signaling in Immunity and Cancer.* Immunity, 2019. **50**(4): p. 924-940 DOI: 10.1016/j.immuni.2019.03.024.
63. Pontiggia, O., et al., *The tumor microenvironment modulates tamoxifen resistance in breast cancer: a role for soluble stromal factors and fibronectin through β1 integrin.* Breast Cancer Res Treat, 2012. **133**(2): p. 459-71 DOI: 10.1007/s10549-011-1766-x.
64. Shekhar, M.P., et al., *Direct involvement of breast tumor fibroblasts in the modulation of tamoxifen sensitivity.* Am J Pathol, 2007. **170**(5): p. 1546-60 DOI: 10.2353/ajpath.2007.061004.
65. Sun, X., et al., *IL-6 secreted by cancer-associated fibroblasts induces tamoxifen resistance in luminal breast cancer.* Oncogene, 2014 DOI: 10.1038/onc.2014.158.
66. Kinoshita, T., et al., *Forkhead box P3 regulatory T cells coexisting with cancer associated fibroblasts are correlated with a poor outcome in lung adenocarcinoma.* Cancer Sci, 2013. **104**(4): p. 409-15 DOI: 10.1111/cas.12099.
67. Li, T., et al., *Colorectal carcinoma-derived fibroblasts modulate natural killer cell phenotype and antitumor cytotoxicity.* Med Oncol, 2013. **30**(3): p. 663 DOI: 10.1007/s12032-013-0663-z.
68. Shen, C.C., et al., *WNT16B from ovarian fibroblasts induces differentiation of regulatory T cells through β-catenin signal in dendritic cells.* Int J Mol Sci, 2014. **15**(7): p. 12928-39 DOI: 10.3390/ijms150712928.
69. Takahashi, H., et al., *Cancer-associated fibroblasts promote an immunosuppressive microenvironment through the induction and accumulation of protumoral macrophages.* Oncotarget, 2017. **8**(5): p. 8633-8647 DOI: 10.18632/oncotarget.14374.
70. Ziani, L., S. Chouaib, and J. Thiery, *Alteration of the Antitumor Immune Response by Cancer-Associated Fibroblasts.* Front Immunol, 2018. **9**: p. 414 DOI: 10.3389/fimmu.2018.00414.
71. Griguolo, G., et al., *Immune microenvironment and intrinsic subtyping in hormone receptor-positive/HER2-negative breast cancer.* NPJ Breast Cancer, 2021. **7**(1): p. 12 DOI: 10.1038/s41523-021-00223-x.
72. Hammerl, D., et al., *Breast cancer genomics and immuno-oncological markers to guide immune therapies.* Semin Cancer Biol, 2018. **52**(Pt 2): p. 178-188 DOI: 10.1016/j.semcancer.2017.11.003.
73. Segovia-Mendoza, M. and J. Morales-Montor, *Immune Tumor Microenvironment in Breast Cancer and the Participation of Estrogen and Its Receptors in Cancer Physiopathology.* Front Immunol, 2019. **10**: p. 348 DOI: 10.3389/fimmu.2019.00348.
74. Nelson, D.J., et al., *A review of the importance of immune responses in luminal B breast cancer.* Oncoimmunology, 2017. **6**(3): p. e1282590 DOI: 10.1080/2162402x.2017.1282590.
75. Tekpli, X., et al., *An independent poor-prognosis subtype of breast cancer defined by a distinct tumor immune microenvironment.* Nat Commun, 2019. **10**(1): p. 5499 DOI: 10.1038/s41467-019-13329-5.
76. Larionova, I., et al., *Tumor-Associated Macrophages in Human Breast, Colorectal, Lung, Ovarian and Prostate Cancers.* 2020. **10**(2232) DOI: 10.3389/fonc.2020.566511.
77. Qiu, S.Q., et al., *Tumor-associated macrophages in breast cancer: Innocent bystander or important player?* Cancer Treat Rev, 2018. **70**: p. 178-189 DOI: 10.1016/j.ctrv.2018.08.010.
78. Gatti-Mays, M.E., et al., *If we build it they will come: targeting the immune response to breast cancer.* NPJ Breast Cancer, 2019. **5**: p. 37 DOI: 10.1038/s41523-019-0133-7.

79. Sadeghalvad, M., H.R. Mohammadi-Motlagh, and N. Rezaei, *Immune microenvironment in different molecular subtypes of ductal breast carcinoma.* Breast Cancer Res Treat, 2021. **185**(2): p. 261-279 DOI: 10.1007/s10549-020-05954-2.
80. Imamura, Y., et al., *Comparison of 2D- and 3D-culture models as drug-testing platforms in breast cancer.* Oncol Rep, 2015. **33**(4): p. 1837-43 DOI: 10.3892/or.2015.3767.
81. Bahcecioglu, G., et al., *Breast cancer models: Engineering the tumor microenvironment.* Acta Biomater, 2020. **106**: p. 1-21 DOI: 10.1016/j.actbio.2020.02.006.
82. Pinto, B., et al., *Three-Dimensional Spheroids as In Vitro Preclinical Models for Cancer Research.* Pharmaceutics, 2020. **12**(12) DOI: 10.3390/pharmaceutics12121186.
83. Han, S.J., S. Kwon, and K.S. Kim, *Challenges of applying multicellular tumor spheroids in preclinical phase.* Cancer Cell Int, 2021. **21**(1): p. 152 DOI: 10.1186/s12935-021-01853-8.
84. Roberts, S., S. Peyman, and V. Speirs, *Current and Emerging 3D Models to Study Breast Cancer*, in *Breast Cancer Metastasis and Drug Resistance: Challenges and Progress*, A. Ahmad, Editor. 2019, Springer International Publishing: Cham. p. 413-427.
85. Van Zundert, I., B. Fortuni, and S. Rocha, *From 2D to 3D Cancer Cell Models-The Enigmas of Drug Delivery Research.* Nanomaterials (Basel), 2020. **10**(11) DOI: 10.3390/nano10112236.
86. Leonard, F. and B. Godin, *3D In Vitro Model for Breast Cancer Research Using Magnetic Levitation and Bioprinting Method.* Methods Mol Biol, 2016. **1406**: p. 239-51 DOI: 10.1007/978-1-4939-3444-7_21.
87. Sasmita, A. and Y. Wong, *Organoids as Reliable Breast Cancer Study Models: An Update.* 2018. **1**: p. 008 DOI: 10.23937/ijor-2017/1710008.
88. de Souza, N., *Organoids.* Nature Methods, 2018. **15**(1): p. 23-23 DOI: 10.1038/nmeth.4576.
89. Tuveson, D. and H. Clevers, *Cancer modeling meets human organoid technology.* Science, 2019. **364**(6444): p. 952-955 DOI: 10.1126/science.aaw6985.
90. Walsh, A.J., et al., *Drug response in organoids generated from frozen primary tumor tissues.* Sci Rep, 2016. **6**: p. 18889 DOI: 10.1038/srep18889.
91. Yuki, K., et al., *Organoid Models of Tumor Immunology.* Trends Immunol, 2020. **41**(8): p. 652-664 DOI: 10.1016/j.it.2020.06.010.
92. Aisenbrey, E.A. and W.L. Murphy, *Synthetic alternatives to Matrigel.* Nat Rev Mater, 2020. **5**(7): p. 539-551 DOI: 10.1038/s41578-020-0199-8.
93. Cardoso, A.P., et al., *Macrophages stimulate gastric and colorectal cancer invasion through EGFR Y1086, c-Src, Erk1/2 and Akt phosphorylation and smallGTPase activity.* Oncogene, 2014. **33**(16): p. 2123-2133 DOI: 10.1038/onc.2013.154.
94. Technologies, S. *RosetteSep™ Human Monocyte Enrichment Cocktail*. 2021 08/08/2021]; Available from: https://www.stemcell.com/products/rosettesep-human-monocyte-enrichment-cocktail.html.
95. Bauleth-Ramos, T., et al., *Colorectal cancer triple co-culture spheroid model to assess the biocompatibility and anticancer properties of polymeric nanoparticles.* J Control Release, 2020. **323**: p. 398-411 DOI: 10.1016/j.jconrel.2020.04.025.
96. Garizo, A.R., et al., *p28-functionalized PLGA nanoparticles loaded with gefitinib reduce tumor burden and metastases formation on lung cancer.* J Control Release, 2021. **337**: p. 329-342 DOI: 10.1016/j.jconrel.2021.07.035.
97. Comşa, Ş., A.M. Cîmpean, and M. Raica, *The Story of MCF-7 Breast Cancer Cell Line: 40 years of Experience in Research.* Anticancer Res, 2015. **35**(6): p. 3147-54.
98. Costa, E.C., et al., *3D tumor spheroids: an overview on the tools and techniques used for their analysis.* Biotechnol Adv, 2016. **34**(8): p. 1427-1441 DOI: 10.1016/j.biotechadv.2016.11.002.
99. Weiswald, L.B., D. Bellet, and V. Dangles-Marie, *Spherical cancer models in tumor biology.* Neoplasia, 2015. **17**(1): p. 1-15 DOI: 10.1016/j.neo.2014.12.004.

100. Ivanov, D.P. and A.M. Grabowska, *In Vitro Tissue Microarrays for Quick and Efficient Spheroid Characterization.* SLAS Discov, 2018. **23**(2): p. 211-217 DOI: 10.1177/2472555217740576.
101. Elmore, S.A., et al., *Recommendations from the INHAND Apoptosis/Necrosis Working Group.* Toxicol Pathol, 2016. **44**(2): p. 173-88 DOI: 10.1177/0192623315625859.
102. Ham, S.L., et al., *Three-dimensional tumor model mimics stromal - breast cancer cells signaling.* Oncotarget, 2018. **9**(1): p. 249-267 DOI: 10.18632/oncotarget.22922.
103. Sahai, E., et al., *A framework for advancing our understanding of cancer-associated fibroblasts.* Nat Rev Cancer, 2020. **20**(3): p. 174-186 DOI: 10.1038/s41568-019-0238-1.
104. Yakavets, I., et al., *Advanced co-culture 3D breast cancer model for investigation of fibrosis induced by external stimuli: optimization study.* Sci Rep, 2020. **10**(1): p. 21273 DOI: 10.1038/s41598-020-78087-7.
105. Marsh, T., K. Pietras, and S.S. McAllister, *Fibroblasts as architects of cancer pathogenesis.* Biochim Biophys Acta, 2013. **1832**(7): p. 1070-8 DOI: 10.1016/j.bbadis.2012.10.013.
106. Dish, C.C. *T Cell Media: A Comprehensive Guide to Key Components*. 2018 06/09/2021]; Available from: https://cellculturedish.com/t-cell-media-comprehensive-guide-key-components/.
107. Hyun, K.A., et al., *Epithelial-to-mesenchymal transition leads to loss of EpCAM and different physical properties in circulating tumor cells from metastatic breast cancer.* Oncotarget, 2016. **7**(17): p. 24677-87 DOI: 10.18632/oncotarget.8250.
108. Jeong, H., et al., *Tumor-Associated Macrophages as Potential Prognostic Biomarkers of Invasive Breast Cancer.* J Breast Cancer, 2019. **22**(1): p. 38-51 DOI: 10.4048/jbc.2019.22.e5.
109. Scientific, T.F. *LIVE/DEAD™ Viability/Cytotoxicity Kit, for mammalian cells*. 2021 10/08/2021]; Available from: https://www.thermofisher.com/order/catalog/product/L3224?ef_id=CjwKCAjw4KyJBhAbEiwAaAQbExsUfTLRSYtkdODi68VXob7GIDjMuaiqU46zMhKWBgmc-ClvmzdRFhoC3q4QAvD_BwE:G:s&s_kwcid=AL!3652!3!447292198772!b!!g!!&cid=bid_pca_iva_r01_co_cp1359_pjt0000_bid00000_0se_gaw_dy_pur_con&gclid=CjwKCAjw4KyJBhAbEiwAaAQbExsUfTLRSYtkdODi68VXob7GIDjMuaiqU46zMhKWBgmc-ClvmzdRFhoC3q4QAvD_BwE#/L3224?ef_id=CjwKCAjw4KyJBhAbEiwAaAQbExsUfTLRSYtkdODi68VXob7GIDjMuaiqU46zMhKWBgmc-ClvmzdRFhoC3q4QAvD_BwE:G:s&s_kwcid=AL!3652!3!447292198772!b!!g!!&cid=bid_pca_iva_r01_co_cp1359_pjt0000_bid00000_0se_gaw_dy_pur_con&gclid=CjwKCAjw4KyJBhAbEiwAaAQbExsUfTLRSYtkdODi68VXob7GIDjMuaiqU46zMhKWBgmc-ClvmzdRFhoC3q4QAvD_BwE.
110. Gong, X., et al., *Generation of Multicellular Tumor Spheroids with Microwell-Based Agarose Scaffolds for Drug Testing.* PLoS One, 2015. **10**(6): p. e0130348 DOI: 10.1371/journal.pone.0130348.
111. Liu, Z.G. and D. Jiao, *Necroptosis, tumor necrosis and tumorigenesis.* Cell Stress, 2019. **4**(1): p. 1-8 DOI: 10.15698/cst2020.01.208.
112. Monteiro, M.V., et al., *Hydrogel 3D in vitro tumor models for screening cell aggregation mediated drug response.* Biomater Sci, 2020. **8**(7): p. 1855-1864 DOI: 10.1039/c9bm02075f.
113. Däster, S., et al., *Induction of hypoxia and necrosis in multicellular tumor spheroids is associated with resistance to chemotherapy treatment.* Oncotarget, 2017. **8**(1): p. 1725-1736 DOI: 10.18632/oncotarget.13857.
114. To, W.S. and K.S. Midwood, *Plasma and cellular fibronectin: distinct and independent functions during tissue repair.* Fibrogenesis Tissue Repair, 2011. **4**: p. 21 DOI: 10.1186/1755-1536-4-21.

115. Andersen, A.P., et al., *Roles of acid-extruding ion transporters in regulation of breast cancer cell growth in a 3-dimensional microenvironment.* Mol Cancer, 2016. **15**(1): p. 45 DOI: 10.1186/s12943-016-0528-0.
116. Madsen, N.H., et al., *Monocyte Infiltration and Differentiation in 3D Multicellular Spheroid Cancer Models.* Pathogens, 2021. **10**(8) DOI: 10.3390/pathogens10080969.
117. Lee, D. and C. Cha, *The Combined Effects of Co-Culture and Substrate Mechanics on 3D Tumor Spheroid Formation within Microgels Prepared via Flow-Focusing Microfluidic Fabrication.* Pharmaceutics, 2018. **10**(4) DOI: 10.3390/pharmaceutics10040229.
118. del Giglio, A. and C. Ito, *Gefitinib (Iressa) in metastatic patients with non-small cell lung cancer: preliminary experience in a Brazilian center.* Sao Paulo Med J, 2004. **122**(3): p. 128-30 DOI: 10.1590/s1516-31802004000300010.
119. Cohen, M.H., et al., *FDA drug approval summary: gefitinib (ZD1839) (Iressa) tablets.* Oncologist, 2003. **8**(4): p. 303-6 DOI: 10.1634/theoncologist.8-4-303.
120. Manupati, K., et al., *Inhibiting epidermal growth factor receptor signalling potentiates mesenchymal-epithelial transition of breast cancer stem cells and their responsiveness to anticancer drugs.* Febs j, 2017. **284**(12): p. 1830-1854 DOI: 10.1111/febs.14084.
121. Ibrahim, W.N., L. Muizzuddin Bin Mohd Rosli, and A.A. Doolaanea, *Formulation, Cellular Uptake and Cytotoxicity of Thymoquinone-Loaded PLGA Nanoparticles in Malignant Melanoma Cancer Cells.* Int J Nanomedicine, 2020. **15**: p. 8059-8074 DOI: 10.2147/ijn.S269340.
122. Forest, V., M. Cottier, and J. Pourchez, *Electrostatic interactions favor the binding of positive nanoparticles on cells: A reductive theory.* Nano Today, 2015. **10**(6): p. 677-680 DOI: 10.1016/j.nantod.2015.07.002.
123. Schweiger, C., et al., *Quantification of the internalization patterns of superparamagnetic iron oxide nanoparticles with opposite charge.* J Nanobiotechnology, 2012. **10**: p. 28 DOI: 10.1186/1477-3155-10-28.
124. Zhang, X., et al., *Mechanisms of Gefitinib-mediated reversal of tamoxifen resistance in MCF-7 breast cancer cells by inducing ERα re-expression.* Sci Rep, 2015. **5**: p. 7835 DOI: 10.1038/srep07835.
125. Institute, J. *Cytotoxicity Testing According to EN ISO 10993-5: Avoiding Pitfalls When Choosing a Laboratory*. 2021 02/10/2021]; Available from: https://www.johner-institute.com/articles/product-development/and-more/cytotoxicity-testing-according-to-en-iso-10993-5/.
126. Tchoryk, A., et al., *Penetration and Uptake of Nanoparticles in 3D Tumor Spheroids.* Bioconjug Chem, 2019. **30**(5): p. 1371-1384 DOI: 10.1021/acs.bioconjchem.9b00136.
127. Gustafson, H.H., et al., *Nanoparticle Uptake: The Phagocyte Problem.* Nano today, 2015. **10**(4): p. 487-510 DOI: 10.1016/j.nantod.2015.06.006.
128. Ni, Y., et al., *The Role of Tumor-Stroma Interactions in Drug Resistance Within Tumor Microenvironment.* Front Cell Dev Biol, 2021. **9**: p. 637675 DOI: 10.3389/fcell.2021.637675.
129. Changavi, A.A., A. Shashikala, and A.S. Ramji, *Epidermal Growth Factor Receptor Expression in Triple Negative and Nontriple Negative Breast Carcinomas.* J Lab Physicians, 2015. **7**(2): p. 79-83 DOI: 10.4103/0974-2727.163129.